Late Pleistocene glacial terminations accelerated by proglacial lakes

Meike D. W. Scherrenberg[1], Constantijn J. Berends[1], Roderik S.W. van de Wal[1,2]

[1]Institute for Marine and Atmospheric research Utrecht, Utrecht University, 3584 CC Utrecht, the Netherlands
[2]Faculty of Geosciences, Department of Physical Geography, Utrecht University, Utrecht, the Netherlands

5 *Correspondence to*: M.D.W. Scherrenberg (M.D.W.Scherrenberg@uu.nl)

Abstract. During the glacial cycles of the past 800 thousand years, Eurasia and North America were periodically covered by large ice sheets~~.~~ causing up to 100 meters of sea level change. While the Late Pleistocene glacial cycles typically lasted 80 – 120 thousand years, the termination phases only took 10 thousand years to complete. During these glacial terminations, the North American and Eurasian ice sheets retreated which created large proglacial lakes in front of the ice sheet margin.

10 Proglacial lakes accelerate the deglaciation as they can facilitate ice shelves in the southern margins of the North American and the Eurasian ice sheets. ~~Ice~~These ice shelves are characterized by basal melting, low surface elevations and negligible friction at the base. Here we use an ice-sheet model to quantify the ~~effect~~(combined) effects of proglacial lakes~~, and~~ on the ~~combined effect~~Late Pleistocene glacial terminations through their interplay with glacial isostatic adjustment (GIA) ~~on Late Pleistocene glacial terminations.~~

15 and basal sliding. We find that proglacial lakes accelerate the deglaciation of the ice sheets mainly because of the absence of basal friction underneath ice shelves. If the friction underneath grounded ice is applied to floating ice, we find that full deglaciation is postponed by a few millennia, ~~the Barents-Kara Sea region does not fully deglaciate~~more ice remains during interglacial periods, and ~~there are~~ no extensive ice shelves are formed. Additionally, the large uncertainty in melt rates underneath lacustrine ice shelves translates to an uncertainty in the timing of the termination of ~~only a few centuries~~a

20 millennium at most.

Proglacial lakes are created by the depression in the landscape that ~~linger~~remains after the ice sheet has retreated. The depth, size and timing of proglacial lakes depend on the bedrock rebound. We find that if the bedrock rebounds within a few centuries, instead of a few millennia, the mass loss rate of the ice sheet is substantially reduced. This is because fast bedrock rebound prevents the formation of extensive proglacial lakes. Additionally, a decrease in ice thickness is partly compensated

25 by the faster bedrock rebound, resulting in a higher surface elevation with lower temperatures and higher surface mass balance delaying deglaciation. We find that a very long bedrock relaxation time does not affect terminations substantially, but ~~will~~may lead to a later inception of the next glacial period. This is because ~~initial~~ inception regions, such as North-Western Canada, remain below sea level throughout the preceding interglacial period.

1 Introduction

30 From paleoglaciology we can learn which processes are important for the ~~melt~~evolution of ice sheets~~, which~~. This can improve our understanding of the response of the Antarctic and Greenland ice sheets under future warming. During the Late Pleistocene (~800 – 10 thousand years (kyr) ago), the North American and Eurasian continents were recurrently covered by large ice sheets (e.g., Hughes et al., 2015; Batchelor et al., 2019). While a single glacial cycle took on average 80 – 120 kyr, their decay phases only took 10 kyr. The climate underwent global-scale changes during these glacial terminations and sea levels increased by up

35 to 130 meters (Lambeck et al., 2014; Clark and Tarasov, 2014; Simms et al., 2019) mostly due to mass loss of the major ice sheets. As a consequence, the planetary albedo decreased due to the smaller extent of snow, sea ice and ice sheets (~~Clark and Tarasov,~~Abe-Ouchi et al., 2013; Stap et al., 2014). Large volumes of carbon stored in the deep ocean were released (e.g, Denton et al., 2010; Menviel, 2019; Hasenfratz et al., 2019; Sigman et al., 2021) which contributed to an increase in CO_2 concentrations by 80 – 100 parts per million during interglacial periods (Bereiter et al., 2015). These processes and changes in

40 insolation, which are an important pacer for glacial cycles (Milankovitch, 1941), caused global temperatures to increase by roughly 4 – 5 °C (Annan et al., 2022). While each of these processes enhanced the mass loss of the ice sheets, ~~these~~ glaciated regions also ~~act as a positive~~affect the climate and ~~negative feedback in the~~ deglaciation. It has for instance been suggested that the Late Pleistocene deglaciation phases only take place if the ice sheets are large enough (e.g., ~~Abe-Ouchi et al.,2013; Berends et al., 2021; Parrenin and Paillard, 2003).~~Abe-Ouchi et al., 2013; Berends et al., 2021; Parrenin and Paillard, 2003).

45 Additionally, Berends et al. (2021) suggested that this may lead to three ice regimes: a small ice sheet that melts every orbital maximum (e.g., Eurasia, Early-Pleistocene North America), a medium sized that survives orbital maxima through elevation-temperature and albedo-temperature feedbacks (e.g., interstadial North America) and a large ice sheet regime which, due to bedrock-ice feedbacks, becomes sensitive to small increases in summer insolation (e.g. North America at glacial terminations). North America may have undergone a change in size regime during the Mid Pleistocene Transition (MPT; 1.2 Ma – 0.8 Ma),

50 where glacial cycle periodicity shifted from 40 kyr to an average 100 kyr. This shift may have been caused by the removal of regolith during consecutive glacial cycles (e.g., Clark and Pollard, 1998; Tabor and Poulsen, 2016; Willeit et al., 2019), exposing the bedrock underneath and reducing sliding. This results in thicker ice sheets that are less sensitive to insolation maxima and can survive some insolation optima.

There are various ~~ways~~processes controlling the interactions between the ice sheets ~~have a significant impact on~~and

55 the climate and vice versa. Regions with ice and snow have a high albedo, which increases the amount of solar irradiance that is reflected and decreases global and local temperatures. ~~There exists an~~An ice albedo-feedback, where albedo ~~decrease~~decreases due to the retreat of the ice sheets amplifies temperature increase and ablation. Additionally, the elevation of an ice sheet influences the surface mass balance~~; a~~, inducing a positive surface mass balance height feedback. A decrease in surface elevation increases temperatures which enhances ablation and causes a further decrease in ice thickness.

60 ~~Ice~~However, the ice sheet mass balance also depends on the amount of accumulation. The amount of precipitation may decline with elevation as decreasing temperatures lower the vapour pressure and ~~therefore~~ limit the available moisture content.

~~Orographic~~ this leads to a negative feedback. At the same time orographic forcing of precipitation can result in windward and leeward effects, depending on both ice-sheet geometry and prevailing winds. The ice-sheet topography can also influence large-scale atmospheric circulation (Beghin et al., 2015; Löfverström et al., 2016), influencing both temperature and accumulation patterns (Pausata et al., 2011; Ullman et al., ~~2014) on a global scale~~2014; Liakka et al., 2016) on a global scale. Besides melting at the surface, ice sheets can also lose mass at the base. Specifically, water underneath ice shelves can facilitate melting, which can thin ice shelves, thereby reducing buttressing and accelerating ice mass loss. Additionally, mass is also lost at the margin of ocean or lake terminating ice sheets due to calving.

Besides these changes in the forcing, dynamical processes in the ice sheet can also influence the mass loss rates. Marine ice sheets where the grounding line rests on a retrograde slope may exhibit an instability, where a small perturbation can cause a self-sustained advance or retreat (Weertman, 1974; Schoof, 2012). This process is referred to as marine ice sheet instability (MISI) and it is thought to be especially important for the current mass loss in the West-Antarctic ice sheet (Pattyn, 2018), which has substantial parts of its grounding line resting on retrograde slopes. In the past decade, many improvements have been made in capturing MISI in ice-sheet models (e.g, Pattyn et al., 2012, 2013; Schoof, 2007; Schoof, 2012; Sun et al., 2020).

The North American and Eurasian ice sheets ~~had large terrestrial margins. Yet, during glacial terminations these ice sheets~~ may have undergone the lacustrine equivalent of MISI during deglacial phases, called proglacial lake ice sheet instability (PLISI; Quiquet et al., 2021; Hinck et al., 2022). Proglacial lakes are created by the combination of glacial isostatic adjustment (GIA; Peltier, 1974) and runoff. The large mass of the ice sheet prompts bedrock deformation which creates a depression in the landscape. As the ice sheet starts to retreat, the rebound lags behind in time, creating an ice-free depression in front of the ice margin. This depression can fill up with melt water, creating a proglacial lake. Evidence for the existence of large proglacial lakes during the last deglaciation has been found in North America (Lake Agassiz; Upham, 1880; Lepper et al., 2013) and Eurasia (Baltic ice lake; Patton et al., 2017). Besides PLISI, proglacial lakes facilitate the same mass loss processes as marine shelves, though the rates may be different from marine shelves. Lake calving rates are typically at least one magnitude smaller compared to tide-water glaciers (e.g., Warren et al., 1995; Warren and Kirkbride, 2003; Benn et al., 2007). Sub-shelf melting is also different mainly due to the lack of salinity gradients driving sub-shelf circulation under ocean conditions (Sugiyama et al., 2016).

~~Recently,~~The interaction between North America and proglacial lakes has been studied using numerical models (e.g., Tarasov and Peltier, 2006; Hinck et al. ~~(.,~~ 2022~~) and~~, Quiquet et al. ~~(.,~~ 2021 and Austermann et al., 2022). Hinck et al. ~~) have used an ice sheet model to study~~(2022) and Quiquet et al. (2021) studied the effect of PLISI on the deglaciation of North America ~~using PLISI~~. They showed that proglacial lakes significantly accelerate the melt of the ice sheet, with the PLISI-induced mass loss being accelerated by the increased surface melt rates over the low-lying lacustrine shelves. Both studies find that the enhanced retreat by proglacial lakes is not caused by calving or basal melting, but rather due to PLISI and the negative surface mass balance. This is because ice shelves have a low surface elevation with high temperatures and strong ablation.

95   Here, we expand on the work by Hinck et al. (2022) and Quiquet et al. ~~(2021)~~(2021) by considering a wider range of processes related to the presence of proglacial lakes during the deglaciation. We do this by using an ice-sheet model that includes both the North American and Eurasian ice sheets on consecutive glacial cycles. ~~Here, we~~We use an ice-sheet model ~~with a hybrid GCM~~forced by General Circulation Model climate ~~forcing~~time-slices to study the transient effect of proglacial lakes on glacial terminations throughout the Late Pleistocene. Rather than making detailed sea level projections, our main goal

100 is to investigate ice dynamical processes that may have contributed to the melt of the North American and Eurasian ice sheets. ~~Here we investigate~~We focus on the effects of basal sliding, shelf formation, and sub-shelf melting on glacial terminations. ~~We also determined~~In addition, we consider the effect of different GIA response time scales on proglacial lakes and glacial terminations.

2. Methods

105 **2.1 Ice-sheet model**

We simulated the Northern Hemisphere ice sheets using the ~~3-D thermomechanically coupled~~vertically integrated ice-sheet model IMAU-ICE version 2.0 (Berends et al., 2022). The hybrid shallow ice / shallow shelf approximation is used to calculate the flow of ice (Bueler and Brown, 2009). To model GIA, we use an ~~Elastic Lithosphere Relaxing Asthenosphere~~elastic lithosphere relaxing asthenosphere model (ELRA; Le Meur and Huybrechts, 1996). Basal friction is calculated using a Budd-

110 type sliding law (Bueler and van Pelt, 2015~~). The spatially variable bed roughness needed to calculate basal friction is parameterised following the approach of Martin et al. (2011).~~; see Appendix A). We include a simple basal hydrology scheme following Martin et al. (2011), in which pore water pressure depends on ice thickness and the bedrock height compared to sea level. The till friction angle in North America is determined using the geology map from Gowan et al. (2019), which was specifically created for ice sheet model applications. For the Eurasian ice sheet, we generated a till friction angle map based

115 on the sediment thickness map from Laske and Masters (1997), where we use till friction angles of 10 degrees for sediment thicknesses below 100 meters and 30 degrees for thicknesses exceeding that threshold. Basal friction at the grounding-line is treated by a sub-grid friction-scaling scheme (Berends et al., 2022) and is based on the approach used in the Community Ice Sheet Model (CISM; Leguy et al., 2021) and the Parallel Ice Sheet Model (PISM; Feldmann et al., 2014). In this method, the basal friction coefficient of each model grid cell is multiplied with the grounded fraction of that cell. Therefore, friction is

120 decreased were ice is partially floating (grounding line), and is negligible were ice is fully floating (shelves). This grounded fraction is calculated using the approach by Leguy et al. (2021) by bilinearly interpolating the thickness above floatation. Berends et al. (2022) show that the model performs well in the MISMIP and MISMIP+ benchmark experiments, resolving the (migrating) grounding line to within a single grid cell across a range of resolutions.

    Calving is parameterised by a simple thickness threshold scheme, using a threshold thickness of 200 meters. To

125 calculate sub-shelf melt, we use a ~~linear temperature and~~ depth-dependent sub-shelf melt parameterization (Martin et al. ~~2011).~~2011) where the basal melt is linearly related to the anomaly of the temperature. Ocean temperatures are parameterised,

with globally uniform ocean temperature changes (De Boer et al., 2013) which do not capture regional variations in ocean temperatures. We apply the same sub-shelf melting method for oceans and proglacial lakes unless stated otherwise. ~~Lakes and ocean are simulated when the bedrock is below the modelled sea level, an approach similar to Quiquet et al. (2021~~This is a simplification, as the lacustrine and marine environment have different thermal structures, salinity and sub shelf circulation regimes (Sugiyama et al., 2016). Lakes and ocean are simulated when the bedrock is below the modelled sea level. As the ice sheet grows, the bedrock subsides due to GIA. At glacial maxima, large areas of the ice sheet can thus become grounded below sea level. During a deglaciation, the ice sheet retreats and thins, but the bedrock uplift lags the changes in ice load. If the bedrock is below sea level, the cell becomes one of three different types of surfaces: (1) The ice is thick enough that it is grounded and the cell is considered as grounded ice. (2) The ice is thin enough that it can float, and it becomes an ice shelf. (3) There is no ice, and this cell is considered as ocean. There is no distinction between lake and ocean in the model, and processes such as calving and basal melt are treated the same for both, indicating that these processes may be overestimated in the lakes. A further simplification is the constant surface level of the lakes, the consequences of this is explored in paragraph 3.5~~). Hinck et al. (2022), used a lake model that can simulate lake surfaces above sea level. Hinck et al. (2022) showed that retreat is faster with such a lake model rather than the method shown here. Therefore, the effect of proglacial lakes may be underestimated in this study~~.

The North American, Eurasian and Greenland ice sheets are simulated in three separate domains. North America and Eurasia have a 40 x 40 km spatial resolution and Greenland 20 x 20 km. The boundaries of these domains are shown in Fig. 1. The higher resolution of the Greenland ice sheet results in a similar number of grid-cell compared to the other two domains, while capturing smaller topographic features. As shown in Fig. 1, the domains have some overlapping regions. Therefore, regions that appear in more than one model domain are only allowed to have ice in one of them~~;~~, e.g., ice on Ellesmere Island is only simulated in the North American domain but not in the Greenland domain, while ice on Greenland itself is not simulated in the North America domain. We simulate Greenland and North America in separate domains, but they are thought to have ~~merge~~merged during glacial periods.

2.2 Climate forcing

To calculate the melt and accumulation of ice, our surface mass balance model (see section 2.4) requires information on precipitation and temperature as a function of time and space. To obtain the climate forcing computationally efficiently we interpolate between pre-calculated pre-industrial (PI) and last glacial maximum (LGM; 21 kyr ago) time-slices using a matrix method (Pollard et al., 2010). This allows us to implicitly include climate – ice-sheet interactions at low computational costs and ~~is~~forms a good alternative to fully-coupled ice-climate set-ups, which ~~are currently still unfeasible due to the~~have high computational costs. Details of this method, which is based on Berends et al. (2018) and Scherrenberg et al. (2023), are described in appendix ~~C~~B.

~~The matrix method includes a precipitation-topography, albedo-temperature, and elevation-temperature feedback to interpolate between the LGM and PI climate time-slices. Precipitation is calculated based on the local and domain-wide change~~

160 ~~in topography. Therefore, this method implicitly accounts for changes in precipitation resulting from local and large-scale topography changes induced by the ice sheet. Temperature is interpolated with respect to the external forcing and the annual absorbed insolation by the surface, both contributing equally to the interpolation weight in the matrix method. Absorbed insolation is calculated using the ice-sheet model's surface albedo and incoming insolation following the orbital solutions from Laskar et al. (2004). To calculate the annual absorbed insolation index, we interpolate the annual absorbed insolation in the~~

165 ~~model to reference fields calculated using the LGM and PI climate and the corresponding land and ice masks (Abe-Ouchi et al., 2015). To compute the contribution from external forcing, we use a combination of CO_2 and insolation to calculate the external forcing index. Fig. 2 shows how CO_2 (Fig. 2b) and insolation (Fig. 2c) contribute to the external forcing index (~~The main driver of temperature change is the external forcing and the albedo, both contriving 50% to the final temperature interpolation. External forcing is shown in Fig. 2a and is a combination between CO_2 (Fig. 2b; Bereiter et al., 2015) and

170 insolation change (Fig. 2c; Laskar et al., 2004). To derive an interpolation weight from this forcing ~~Fig. 2a). Atmospheric CO_2 is obtained from two different sources, depending on the time period. For the past 800 kyr we use ice-core CO_2 from Bereiter et al. (2015). For time periods before 800 kyr ago, which we use as a spin-up of our simulation, we use leaf-wax proxy-based CO_2 reconstructions from Yamamoto et al. (2022). They have a good agreement with the ice-core record for the overlapping period. To derive a forcing index from both CO_2 and insolation~~, we first determine an index for CO_2, where 0 is LGM (190

175 ppm) and 1 is PI (280 ppm) climate. We then modify this index using the 65°N summer insolation to capture changes in temperature ~~changes~~ caused by the orbital cycles.

~~With stronger (weaker)~~ Therefore, when summer insolation ~~the index is increased (decreased) and~~ decreases the climate forcing becomes closer to ~~PI (~~LGM~~).~~ leading to cooling. The forcing index remains unchanged if the insolation is 440 W/m^2 (see Fig. ~~2a). Finally, the forcing index is capped between -0.25 and 1.25 to prevent too much extrapolation of the~~

180 ~~forcing. The resulting forcing index is shown in~~ 2a and Fig. ~~2. This figure shows that~~ 2c). As a result, for LGM CO_2 concentrations, the forcing index can still be relatively high for strong insolation, and the forcing index for PI CO_2 levels can be relatively low for weak insolation values. ~~The forcing index (a function of time) is then combined with the modelled annual absorbed insolation (a function of time and space) to interpolate the PI and LGM temperatures. Preliminary experiments showed that this computationally efficient method of including insolation changes improves the modelled glacial cycles in~~

185 ~~terms of the timing of deglaciations~~We have tuned the effect of insolation on the forcing index to capture the glacial cycle periodicity across the past 800 thousand years. To calculate the albedo feedback, we multiply the modelled surface albedo with the insolation to obtain the annual amount of insolation absorbed by the surface. We then calculate an interpolation weight from the concurrent amount of absorbed insolation and compare it to the fields obtained with LGM and PI climates and masks. The matrix method includes a precipitation-topography feedback as precipitation is interpolated with respect to the local and

190 domain-wide change in topography relative to the LGM and PI topography.

2.3 Climate time-slices and downscaling

~~When~~By simulating the last glacial cycle using an ice-sheet model, it has been shown that the LGM extent and volume are strongly dependent on the climate forcing (Charbit et al., 2007; Niu et al., 2019, ~~Adler~~Alder and Hostetler, 2019; Scherrenberg et al., 2023). Not all ~~general circulation models (~~GCM~~)~~ simulations can be used to model an LGM ice sheet extent that
195 ~~agree~~agrees well with reconstructions (Scherrenberg et al., 2023; Niu et al., 2019). Here we use the mean of MIROC (Sueyoshi et al., 2013), IPSL (Dufresne et al., 2013), COSMOS (Budich et al., 2010) and MPI (Jungclaus et al., 2012) members of the paleoclimate modelling intercomparison project phase 3 (PMIP3; Braconnot et al., 2011). This ensemble has been shown to yield good LGM extent in combination with IMAU-ICE (Scherrenberg et al., 2023). To correct for biases in the GCM data, we calculate the difference between the PI time-slice and the reanalysis from ERA40 (Uppala et al., 2005). This bias is then
200 applied to both the PI and LGM time-slice. ~~However~~As a consequence, the resulting PI time-slice may contain some of the anthropogenic warming enclosed in ERA40.

The topography and spatial resolution differ between the climate forcing and the ice-sheet model. Therefore, some corrections need to be applied before the climate forcing can be used in IMAU-ICE. First, we bilinearly interpolate the climate forcing to the finer ice-sheet model grid. As the climate forcing has a lower resolution and therefore a smoother topography,
205 some topographic corrections need to be applied to the temperature and precipitation fields. For temperature, we apply a lapse-rate-based correction. For precipitation we use the Roe and Lindzen (2001) model to capture the orographic forcing of precipitation on the sloping ice margin, and the plateau desert effect in the ice-sheet interior. A more detailed description of the bias correction and downscaling methods can be found in appendix ~~B~~C.

2.4 Surface mass balance model

210 The surface mass balance (SMB) is calculated monthly using IMAU-ITM (insolation-temperature model; Berends et al., 2018). For the present-day climate this provides an adequate SMB distribution as shown in the Greenland surface mass balance model intercomparison project (GrSMBMIP; Fettweis et al., 2020). Using this model, accumulation of snow is calculated using the large-scale snow-rain partitioning proposed by Ohmura, (1999). Refreezing is calculated following a scheme by Huybrechts and de Wolde, (1999) and Janssen and Huybrechts, (2000). Ablation is calculated based on Bintanja et al. (2002) and depends
215 on temperature, insolation and albedo. The equations describing this scheme (IMAU-ITM) are discussed in more detail in appendix ~~A~~D.

3. Results

We conducted a "Baseline" by simulating the North American ice sheets from 782 ka to present-day. Fig. ~~We conduct a spin-up experiment where the model simulates the Northern Hemisphere ice sheets during the period from 1450 kyr ago to 800 kyr
220 ago with CO₂ forcing obtained from leaf-wax proxy data by Yamamoto et al. (2022). We then conduct a "Baseline" experiment by continuing this experiment from 800 kyr ago to present-day with CO₂ forcing obtained from ice cores by Bereiter et al.~~

(2015). The total sea-level contribution of this Baseline is shown in Fig. 33a shows the extent of the ice sheets at the LGM compared to a reconstruction by Dalton et al. (2020; orange contours). The modelled LGM extent matches the reconstructions reasonably well, though ice coverage is lacking in the British island. A small proglacial lake is created in North America around 14 kyr ago (Fig. 3d). The North American ice sheet retreats faster compared to the reconstruction from 12 kyr ago onwards (Fig. 3e-g), with full retreat already reached at 10 kyr ago rather than two millennia later. This is likely due to the absence of a feedback between melt water, the ocean and climate. For example, prior to the Younger Dryas (12.9-11.7 kyr ago), large amounts of fresh water would flow into the North Atlantic (Teller et al., 2002; Tarasov and Peltier, 2005, 2006; Condron and Winsor, 2012), which can collapse the Atlantic meridional overturning circulation (AMOC) and would result in cooling (McManus et al., 2004; Velay-Vitow et al., 2024) and a stagnation in sea level rise (Lambeck et al., 2014). At present-day (see Fig. 3i), the North American and Eurasian ice sheets have fully melted, except for some small ice caps in regions that are currently partly glaciated (e.g., Artic Archipelago, Svalbard, Iceland).

The total sea-level contribution of this Baseline simulation is shown in Fig. 4 and compared to ice volume reconstructions by Spratt and Lisiecki (2016), and Grant et al. (2014). Since we only simulate Northern-Hemisphere ice sheets, we added 30% to the ice sheet contribution to account for sea level changes caused by processes other than the Northern-Hemisphere ice sheets, such as the Antarctic and Patagonian ice sheets (Simms et al., 2019). (~10 m), Greenland and Patagonian ice sheets (Simms et al., 2019). While Antarctic ice volume was shown to be correlated to Northern Hemisphere ice volume as sea level change prompts grounding line advance and retreat (Gomez et al., 2020), this approach neglects out of phase behaviour between Northern and Southern Hemisphere ice mass loss.

We find that the modelled sea level matches the reconstructions well and our simulation captures all major melting events throughout except MIS 13 (marine isotope stage; 530-480 kyr ago), which has relatively low atmospheric CO_2 concentrations (~240 - 250 ppm) compared to the Late Pleistocene. The modelled interglacial periods that succeeded it (Siegenthaler et al., 2005; Bereiter et al., 2015). The modelled inception periods are long compared to reconstructions, which may have resultedespecially the warm interglacial MIS 11 (425-375 kyr ago). This results from the PI temperatures. Due to a bias correction based on observations where our PI time-slice shows some anthropogenic warming. ThereforeConsequently, ice inception requires relatively low CO_2 concentrations and weak insolation. Nevertheless, theThe ability of the model to capture the overall pattern of glacial terminations and interglacial periodsfully melting North American and Eurasian ice sheets allows us to study the importance of ice dynamical processes that may have contributed to the decay of the ice sheets.

Fig. 45 shows the total ice volume changes for time-series of North America (Fig. 5b), Eurasia (Fig. 5c) and the Northern Hemisphere (Fig. 4a), North American (Fig. 4c) and Eurasian (Fig. 4e) ice sheets. Blue indicates5a), colours indicating net melt (red), net accumulation (blue), and red indicates net melt of the ice sheets. Red squares have been added to indicatepoints indicating the onset of deglaciations or interstadials. A blue circle. In Fig. 5d-f, the ice volume is added at the start of glaciations or the end of interstadials. These model states are compared to the externalplotted against climate forcing index in Fig. 4b, d, with a glacial climate on the left and f, where an external forcing index of 0 (1) signifies LGM (PI) climate.

255   ~~Obviously, when~~interglacial climate on the right. When the climate becomes colder ~~(warmer)~~ the ice sheet will tend to have a net ~~accumulation (ablation).~~positive mass balance and will grow. However, when the ice sheet becomes larger and grows more towards the warmer south, the ~~climate needs~~CO_2 concentration and insolation need to be ~~colder, or specifically more glacial,~~lower to be able to maintain net ~~accumulation~~growth. This agrees with Abe-Ouchi et al. (2013) and Parrenin and Paillard (2003) and shows that a larger ice sheet ~~is~~will be more vulnerable to ~~a decay. Once the~~increases in

260 insolation, and that deglaciations tend to take place when ice volume is large enough.

The Eurasian ice sheet ~~reaches LGM volume, any additional cooling barely increases the size of the ice sheet. This may partly result from the precipitation-topography feedback implemented in the model. As the ice sheet becomes larger, the climate becomes more arid and less moisture is available to grow the ice sheet. At the same time the ice sheet size at LGM is somewhat constrained by the fact that large marginal regions border the ocean which prevents further lateral extension.~~

265   ~~Furthermore, the~~ Eurasian ice sheet ~~(Fig. 4f)~~ is more sensitive to ~~insolation and CO₂ increases~~collapse compared to the North American ice sheet ~~(Fig. 4d). The same.~~ Occasionally, the Eurasian ice sheet melts completely (e.g.,168 kyr ago, 50 kyr ago), while the North American ice sheet only undergoes partial melt. This suggest that the Eurasian ice sheet is more vulnerable to complete melt during climate optima and that CO_2 concentrations and insolation can facilitate decay of the Eurasian ice sheet and at the same time be favourable enough for the North American ice sheet to survive ~~at the same time.~~an

270 interglacial. On average, Eurasia achieves full deglaciation roughly three millennia earlier compared to the North American ice sheet.

     This is in line with Bonelli et al. (2009~~) and~~), Abe-Ouchi et al. (2013), ~~both~~and Tarasov and Peltier (1997b), finding that the Eurasian ice sheet needs lower CO_2 concentrations ~~and~~or insolation compared to the North American ice sheet~~.~~ to survive climatic optima. The higher sensitivity of the Eurasian ice sheet also follows from ice ~~volume~~ reconstructions, such as

275 Gowan et al. (2021) and Mangerud et al. (2023), who show that the Eurasian ice sheet lost most of its volume during the ~~MIS3~~MIS 3 (60-25 kyr ago) interstadial, while the North American ice sheet continued to survive until the LGM. This higher sensitivity for Eurasia to melt during a climate optimum may in part be due to the smaller size: Eurasian sea level contribution at LGM is 19.1 m, compared to 80.1 m for North America, and higher LGM temperatures in the climate forcing, resulting largely from the thinner Eurasian ice sheet.

280 3.1 Design of the perturbed experiments

To investigate the effect of proglacial lakes and GIA on the Late Pleistocene terminations, we carry out a set of experiments that are similar to the Baseline experiment, but have one process ~~altered~~changed at a time. In the Baseline set-up, our model reproduces the basic features of glacial terminations throughout the Late-Pleistocene. For the sensitivity experiments, we modify the Baseline simulation to investigate the effect of sub-shelf melting, basal friction of grounded ice, sub-shelf basal

285 friction and GIA on the deglaciation of the Northern Hemisphere ice sheets. Each simulation branches off from the Baseline simulation at 782 kyr ago, which is during an interglacial period when the North American and Eurasian continents were mostly ice-free. In the next few sections, we introduce these perturbation experiments to investigate which processes are

important for ~~melting~~the decay of the ice sheets. These experiments are described in paragraphs 3.2-3.~~5~~6 and summarized in Table 1.

290

Table 1: A description of the experiments. Each perturbed experiment is similar to the Baseline except for the described feature.

Experiment	Description	Section
Low Friction	Till friction angle is set to 10 degrees, representing full sediment coverage	3.2
High Friction	Till friction angle is set to 30 degrees, representing full bedrock coverage	3.2
Zero BMB	Basal mass balance is set to 0 everywhere	3.~~2~~3
Rough Water	The basal friction of floating ice is the same as land	3.~~3~~4
Lake 100m	Increased lake levels in North America by 100 m	3.5
Lake 200m	Increased lake levels in North America by 200 m	3.5
Lake 300m	Increased lake levels in North America by 300 m	3.5
Lake 400m	Increased lake levels in North America by 400 m	3.5
Fast GIA	~~The~~ GIA relaxation time ~~is decreased from 3,000 to~~of 300 years	3.~~4~~6
Slow GIA	~~The~~ GIA relaxation time ~~is increased from 3,000 to~~of 10,000 years	3.~~4~~6

3.2 The effect of basal friction of grounded ice

The till friction angle is prescribed and based on the geological map (Gowan et al., 2019; North America) and sediment map (Laske and Masters, 1997; Eurasia). To assess the impact of basal friction on the deglaciation, we conducted two sensitivity experiments. First, the Low Friction simulation where till friction angles are set to 10 degrees over the entire North American and Eurasian domains and is a rough representation of continents fully covered by sediments, which are easily deformed. Secondly, the High Friction simulation roughly represents full bedrock coverage where the till friction angles are set to 30 degrees. The basal hydrology is applied the same for all till friction angle maps and does not distinguish between sediment or bedrock.

Fig. 6 shows a time-series of the global mean sea level contribution for the Low Friction, Baseline and High Friction experiments. Panels b-k zoom in on individual glacial terminations. The basal friction has a substantial impact on the deglaciation. As shown in Fig. 6, decreasing till friction angle always results in an earlier completed deglaciation. In the Low Friction simulation, the peak melt ~~on~~ rate in North America is achieved an average four centuries earlier compared to the Baseline, while for the High Friction simulation, the peak mass loss rate is achieved a millennium later (see Fig. S1, S2). In the Low Friction scenario, the ice sheet does fully melt at MIS 13, while in the High Friction full deglaciation is not reached at either MIS 13 and MIS 17 (712 – 676 kyr ago).

Increasing friction will also lead to increased ice volume at glacial maxima, though ice extent is not impacted as much. At the LGM, North American global mean seal level contribution in High Friction is 93.6 m (17% larger) compared to

the Baseline (80.1 m), while Low Friction has a contribution of 75.3 m (6% smaller). Similarly, the Eurasian sea level contribution at LGM is 19.1 m for the Baseline, 18.8 m for Low Friction and 23.7 m for High Friction. Fig. 7, shows maps with ice thickness for the Baseline, Low Friction and High Friction. Ice area at the LGM (Fig.7 a,f,k) deviates less than 1% for North America and 3% for Eurasia between each simulation. Additional ice volume therefore mostly results from the increase in thickness (see Fig.7a,f,k). A time-series comparing ice volume and area over the entire Late Pleistocene is shown in Fig. S3.

These results suggest that basal friction has a large influence on melt rates during climate optima. Lower friction results in thinner ice sheet with gentler slopes, a large ablation area and lower SMB. Combined with increased ice velocities transporting more ice towards the ablation area, these processes can explain the increased sensitivity of the ice sheet during deglaciations and interstadial periods. As friction is reduced, the ice sheet may become more sensitive to collapse during climate optima, which is at the base of the regolith hypothesis, where the MPT may be explained by an increase in basal drag as sediment has been gradually removed during glacial cycles.

First of all, proglacialTo study the robustness of our results, we also conducted the Low Friction and High Friction experiments with the set-up used for the Rough Water and Fast GIA simulations discussed in section 3.4 and 3.6 (see Fig. S4, S5).

3.3 The effect of basal melt on glacial cycles

Proglacial lakes facilitate ice shelves, which can undergo sub-shelf melting. Sub-shelf melting is considered an important process for the current mass-loss of Antarctica (Pritchard et al., 2012; Shepherd et al., 2018). While), where sub-shelf melting underneath Antarctica's shelves is dominated by temperature and salinity gradients,. Lake Agassiz was a fresh water lake created by the melting ice sheet. Therefore and could therefore have substantially reduced basal melt rates compared to parameterizations made for ocean shelves. Here, we conduct a sensitivity test to investigate ifwhether sub-shelf melting could havehas a significant impact on the retreat of the North American and Eurasian ice sheets.

The Zero BMB experiment deviates from the Baseline by setting the sub-shelf melt rate in North America and Eurasia to 0. Fig. 58 shows the ice-volume time-series calculated in the Zero BMB experiment and compares it to the Baseline. Fig. 5b8b-k show the terminations in more detail. Zero BMB is similar to the Baseline, though the ice sheets during glacial periods are slightly bigger. However, the Zero BMB has only a small effect on the glacial terminations, delaying full deglaciation by up to a few centuries. and shelves can extent far into the ocean. During most terminations removing sub-shelf melting only has a small effect, delaying full deglaciation by up to a millennium. MIS 13 and MIS 17 are exceptions. In MIS 17, substantially less ice is melted in the Zero BMB experiment compared to the Baseline, with lowest Northern Hemisphere sea level contribution reaching 15.9 m in the Zero BMB and 4.0 m in the Baseline. Contrarywise, more ice is lost during MIS 13 in the Zero BMB simulation, despite the lack of sub-shelf melting. This is caused by the increased sensitivity of the ice sheets when ice volume is higher, as is shown in the relationship between ice sheet decay and climate forcing in Fig. 5. The Zero BMB has

a substantially larger ice volume during the glacial period preceding MIS 13, and the retreat produces a substantial proglacial lake while the Baseline does not (see Fig. S6).

3.~~3~~4 The effect of basal friction of floating ice

The ice shelves floating on proglacial lakes or seas experience negligible basal friction, which results in relatively high flow

345 velocities. To study the impact of this lack of friction, we conduct the Rough Water experiment ~~where~~. In this experiment the sub-grid friction coefficient ~~of ocean/lake water~~ is not ~~set to zero~~scaled with the grounded fraction, but is instead ~~is~~ calculated as if ~~the ice were grounded.~~all grid cells are grounded. Therefore, friction under shelves is not negligible any more. This essentially prevents the formation of shelves, so that a migration of the ~~groundling~~grounding line will not cause a change in friction, which prevents PLISI/MISI. While this is a very unrealistic scenario, the ~~groundling~~grounding line does not migrate

350 far into the ocean to cover the entire ice domain due to strong ablation~~.~~, which can be seen in the ice thickness and bedrock topography maps in Fig. 9i-l.

The sea level contribution for the Rough Water experiment ~~can also be found~~shown in Fig. ~~5 and is~~8 can be compared to Zero BMB and the Baseline. During the onset of the termination, the Rough Water experiment losses mass at roughly the same pace as the Baseline. However, once more than half of the ice volume is lost, the mass loss rate in Rough Water slows

355 down with respect to the Baseline. This is because the proglacial lakes are only created once the ice sheet has already partly retreated. Therefore, while the Baseline and Rough Water experiments have a similar retreat rate at the onset of the termination, the retreat in the Baseline simulation accelerates once the proglacial lake has formed. Further differences between the Rough Water and Baseline can be seen in ~~Fig. 6a-d, which shows a transect of the North American ice sheet at 11 kyr ago.~~the transect shown in Fig. 10. While the Baseline simulation has large ice shelves in North America, almost the entire ice sheet is grounded

360 in the Rough Water simulation. The shelves in the Baseline have large ice velocities due to the negligible sub-shelf friction. ~~Consequentially~~Consequently, the surfaces of the ice shelves in the Baseline simulation are flat and close to sea level and therefore experience high temperatures and strongly negative SMB. In the Rough Water simulation, these shelves are very small~~, and~~. Without extensive shelves, the higher elevation ~~of the grounded ice results~~and steeper slopes result in a smaller ablation area.

365 ~~Interglacial ~~Fig. 7 compares the forcing index and ~~ice volume ~~foris generally larger in the Rough Water simulation~~. For North America, the threshold for melt is very similar~~ compared to the Baseline~~ simulation. However, the Eurasian ice sheet does not fully melt~~. Eurasia melts completely only during ~~the Rough Water experiment. Instead, the ice dome~~glacial terminations, rather than also during interstadial periods. Additionally, more ice tends to survive interglacial periods in both North America and Eurasia, which can be observed in the Barents-Kara Sea region ~~persist throughout the entire~~

370 ~~Late Pleistocene, suggesting that MISI may be an important process to melting this ice dome. Currently, this region is a shallow sea, surrounded by islands such as Novaya Zemlya ~~and ~~Svalbard that have cold enough climates~~the Arctic Archipelago (see Fig. 9l). These results are sensitive to ~~be partly covered by glaciers. With the high albedo of the Barents-Kara ice dome facilitating lower temperatures~~basal friction though, and ~~without~~an increase in friction can lead to more ice surviving through

interstadial periods. In the High Friction equivalent to the Rough Water experiment neither Eurasia nor North American fully deglaciate, with smallest sea level contributions of 4.5 m and 11.5 m respectively (see Fig. S5).

3.5 Lake Depth

Lakes are assumed to exist in the model wherever the (GIA-adjusted) bedrock is below the modelled sea level, and the modelled ice is thin enough to be floating. In the Baseline experiment, the water level of the modelled lakes is assumed to be equal to sea level, while in reality this can be significantly higher. To assess the effect of ~~MISI, the~~ this simplifying assumption on our results, we simulate the last deglaciation (21 kyr ago – present-day) with a set of four different constant sea levels (Lake 100m, 200 m, 300 m and 400 m) relative to present day. Therefore, lakes are simulated when bedrock is below these fixed sea levels, resulting in increased lake levels. Note that we apply these sea levels on the entire domain, as determining the exact location of lakes requires a high spatial resolution, as lower resolution can smoothen valleys and therefore miss drainage pathways (Berends et al., 2016). The experiments shown here are therefore an overestimation of the melt rates compared to a high resolution lake model which allows for more drainage. Obviously very high sea levels (e.g., 400 m) create an unrealistic inland sea that can hamper glacial inception, so instead we only apply these fixed levels during the last deglaciation and focus on the North American ice sheet only. Despite that, even our most extreme scenario (400 m) does not induce an immediate collapse after the start of the simulation.

A time-series of ice ~~dome may survive insolation and CO₂ maxima~~volume for the four Lake level experiments and the Baseline is shown in Fig. 11a. The evolution of ice extent is shown in Fig. 11b-f, colours indicating when each region of North America was last covered by ice. Here we find that the retreat of the North American ice sheet is much faster with increasing sea level, translating to roughly one millennium lead in terms of ice volume. These results indicate that lake levels are important to the rate of deglaciation for the North American ice sheet and that higher lake levels can substantially accelerate deglaciation.

3.~~4~~6 Glacial isostatic adjustment

Proglacial lakes are created by the interaction between GIA, ice sheets and melt water~~. The large mass of the ice sheet causes~~, and as a ~~depression in the landscape. As the ice sheet retreats, this depression can facilitate a proglacial lake at the ice margin. The~~consequence the GIA relaxation time ~~of the GIA~~controls how ~~fast~~quickly the bedrock fully recovers from a change in ice load. This relaxation time, as well as the thickness of the ice sheet and the retreat rate, ~~may~~control the size and shape of the proglacial lake. Here we assess the effect of GIA ~~by comparing~~response time on multiple glacial cycles while modelling PLISI. We compare three simulations; the previously shown Baseline simulation (3000-yr), the Slow GIA (10,000-yr), and Fast GIA (300-yr relaxation time).

Fig. ~~8~~12 shows the ice volume time-series of these three simulations, with the smaller panels zooming in on individual terminations (Fig. ~~8b-8k~~12b-k). The retreat in the Slow GIA simulation is generally slower, and can lag up to a millennium ~~slower compared to~~behind the Baseline ~~simulation. As~~in terms of ice volume, though some deglaciations have minimal

difference with the ~~ice sheet grows,~~Baseline (e.g., the ~~bedrock subsides. However,~~last and penultimate deglaciations). This could be explained by both difference in bedrock topography at the onset of deglaciations and the proglacial lake. The slower subsidence rates in the Slow GIA~~, the subsidence rate is smaller compared to the Baseline.~~ simulations may result in higher bedrock topographies. This reduces the modelled saturation at the base, as saturation increases with decreasing bedrock topography relative to concurrent sea level. Therefore, ~~at the start of the termination the bedrock~~basal friction may be lower in the Slow GIA ~~is further from equilibrium~~at the onset of some terminations, resulting ~~in higher ice and bedrock topography. Therefore, as the ice sheet starts to~~to reduced retreat ~~the SMB is higher leading to a slower deglaciation.~~rates. However, if the bedrock topography during a glacial maximum is similar to the Baseline, the retreat will be similar as well (see Fig. ~~8j).~~12c,j,k). An exception is MIS 13, were the North American ice sheet in the Slow GIA fully melts while the Baseline does not. Retreat rates and ice sheet volume are not large enough to induce a proglacial lake in the Baseline. However, in the Slow GIA simulation, the slower bedrock uplift allows for a proglacial lake to be created and sustained throughout this termination event, allowing the North American ice sheet to fully melt (see Fig. S6).

The ice thickness and bedrock topography for the Slow GIA simulation are shown in Fig. 9m-p for 21, 12, 10 and 0 kyr ago. The proglacial lakes during retreat are significantly larger compared to the Baseline, as the bedrock uplift is slower. Slow GIA also has a delayed inception phase ~~(see~~which can be seen from Fig. ~~8a).~~12. Due to the slow bedrock uplift, large parts of North America are still below sea level millennia after the ice sheet ~~have~~fully receded~~.~~ (see Fig. 8o). As a result, regions such as North-Eastern Canada, a location for ice inception, are still below sea level throughout the entire preceding interglacial period.

Fast GIA has ~~a~~substantially slower ~~deglaciation~~melt rates compared to the Baseline, Slow GIA, and Rough Water ~~simulation~~simulations, which can be seen in transects shown in Fig. ~~6. Though, on~~10 and the ~~contrary to Rough Water, the Eurasian~~ice ~~sheet can fully melt as MISI is possible~~thickness maps shown in ~~the Barents-Kara Sea region~~Fig. 9q-t. The delayed deglaciation is due to two processes. Firstly, as the ice sheet retreats, the rapid bedrock rebound quickly eliminates the depression ~~that was~~left by the ice sheet, preventing the formation of proglacial lakes~~.~~ (See Fig. 9q-t). Secondly, the ice thickness ~~loss~~decrease is more efficiently compensated by the bedrock rebound, reducing the elevation-temperature feedback and thereby reducing surface melt rates~~.~~ and slowing down the deglaciation. Therefore, while both the Fast GIA and Rough Water eliminate the effect of proglacial lakes, only the Fast GIA reduces melt rates from the onset of the termination. During many interglacial periods – including present-day – an ice dome persists or the termination is skipped. However, this is again strongly dependent on the basal friction, with the Low Friction equivalent of the Fast GIA experiment inducing full melting during most interglacial periods, while the High Friction equivalent never melts completely (see Fig. S4, S5). The combination of the lack of lakes and the SMB-elevation feedback makes the Fast GIA the simulation with the slowest ~~melt shown here~~deglaciation.

4. Discussion

In this study, we investigate the effect of proglacial lakes on the deglaciation of the Eurasian and North American ice sheets throughout the past 800 kyr. In the Baseline configuration, the modelled ice volume over time generally agrees well with different sea-level reconstructions, so that all major deglaciations throughout the Late Pleistocene are captured. However, aA shortcoming is the lack of ice coverage in the British Islands, and that our simulations tend to have slightly too long interglacial periods compared to reconstructions, especially MIS- 11 interglacial which had higher global temperatures and sea-levels compared to present day (Hearty et al., 1999; Raymo and Mitrovica, 2012). Sea levels that are higher than 7.4 meters with respect to present day are not possible as we do not model the Antarctic ice sheet. Warmer than pre-industrial temperatures are also not captured, as our climate forcing was interpolated from PI and LGM time-slices. Therefore, any climate that has both higher CO$_2$ concentrations and summer insolation than PI will require some extrapolation. Adding additional time-slices to our matrix method, similar to Abe-Ouchi et al. (2013),(2013), particular for warmer than present-day conditions may improve our representation of different ice volume, CO$_2$ concentration and orbital parameters. However, as shown by Scherrenberg et al. (2023), the ice sheet extent dependsResults are anyhow depending strongly on the quality of the climate forcing. (Scherrenberg et al., 2023). Here we have chosen a forcing that would result in an LGM extent that agrees well with reconstructions rather than a large number of time-slices.

The size and shape of proglacial lakes follow from the interaction between GIA and ice thickness. Here we have used uniform GIA response times, but in reality, GIA varies spatially (e.g., Forte et al., 2010; van Calcar et al., 2023) and has large uncertainties. GIA can increase the size of proglacial lakes, compared to no GIA (e.g., Austermann et al. 2022), and in this study we have shown that when increasing the GIA response time, proglacial lakes will be larger. A faster GIA response will decrease the size of proglacial lakes, and the increased bedrock uplift can partly compensate thickness loss resulting in reduced melt rates.

Here we have simulated lakes when bedrock is below sea level. This is a simplification, as lakes can exist well above sea level, and as shown in the Lake 100 – 400 m experiments, increasing lake levels will result in a substantially faster deglaciation. In this study we have treated lakes as if they were ocean, but due to the low salinity and smaller size of lakes they can have substantially different sub-shelf melting (Sugiyama et al., 2016), lower calving rates (e.g., Warren et al., 1995; Warren and Kirkbride, 2003; Benn et al., 2007), and the clogging of icebergs can create a potential buttressing effect (Geirsdóttir et al., 2008). These limitations suggest that the effect of basal melt and calving may be overestimated in the proglacial lakes. These limitations are further enforced by uncertainties in the sub-shelf melting and calving schemes used here. For example, applying a more sophisticated sub-shelf melting scheme, which simulates high melt rates near the grounding line (Rignot and Jacobs, 2002), may result in a greater impact from sub-shelf melting. Additionally, here we have not explored the effect of calving rates in detail, but lake calving can have an effect on ice flow of the Laurentide ice sheet (e.g., Cutler et al., 2001). Nevertheless, our results suggest that while sub-shelf melting can enhance melt of the North American and Eurasian ice sheet, it is overshadowed by large surface melt rates combined with PLISI. Due to these limitations, we cannot give an exact estimate

470 to how much longer a deglaciation phase will take when removing sub-shelf melting, but it serves as an indication that full melt can take place without sub-shelf melting.

Another limitation is the treatment of basal friction. For basal hydrology we have used a parameterization from Martin et al. (2011), and till friction angle was based on geology and sediment masks. We performed experiments by decreasing the till friction angle to 10 or 30 degrees representing a full sediment cover or full hard bed coverage. We found that these have a

475 substantial influence on the ice volume at glacial maxima, with a much smaller effect on the extent. Deglaciation is also slower with increasing friction. While our main conclusions are consistent regardless of basal friction, the timing of deglaciation and the ice volume that persists through interglacial periods differ substantially. This highlights that glacial cycle volume and melt rates are sensitive to the basal friction. Here we have used a static till friction angle mask. However, friction can change over time as bedrock is eroded and sediment is transported. Basal friction can therefore be improved by including a sediment

480 transport model (e.g, Hildes et al., 2004; Melanson et al., 2013), combined with a more sophisticated basal hydrology method (e.g., Hoffman and Price, 2014; Flowers, 2015).

The matrix method, which we use to interpolate between the LGM and PI time-slices, implicitly includes a temperature-albedo and precipitation-topography feedback. However, ice-sheet climate interactions can exhibit threshold behaviours which cannot be simulated using our method. For example, the opening and closing of straits such as the Canadian

485 Arctic Archipelago (Löfverström et al., 2022) or the response of Heinrich and Dansgaard/Oeschger events (Claussen et al., 2003), or rapid changes in ocean circulation and sea ice due to the influx of melt water into the ocean (Otto-Bliesner and Brady, 2010). Additionally, since we do not model the ocean, there isare no interactions between melt water and, ocean circulation. and the climate. This may explain why the Baseline simulation has too high retreat rates from 12 kyr ago, coinciding with the Younger Dryas. The Younger Dryas has reduced rates of sea level rise (e.g., Lambeck et al., 2014) and lower Northern

490 Hemisphere temperatures due to a stagnation of the AMOC (McManus et al., 2004; Velay-Vitow et al., 2024) which was likely caused by an influx of melt water into the North Atlantic (Teller et al., 2002; Tarasov and Peltier, 2005, 2006; Condron and Winsor, 2012). This process is not included in our set-up as temperature is only affected by CO_2, insolation, elevation and albedo, and therefore fail to capture the stagnation in melt rates during the Younger Dryas.

Including many of these threshold behaviours would require a model that more explicitly simulates the climate

495 system. GCM models may be able to simulate these interactions, but simulating glacial cycles is unfeasible as it requireswith a too largereasonably high resolution would require an excessive amount of computational resources. ThoughAlternatively, ocean-atmosphere circulation models can be used to simulate individual glacial terminations (Obase et al., 2021). Alternatively,), or intermediate complexity models (Ganopolski and Calov., 2011) can simulate multiple glacial cycles with more explicitly calculateexplicit feedbacks in the climate system, though still at highhigher computational costs than ice sheet

500 models, and with more parameterizations compared to full GCMs.

5. Conclusion

We ~~have~~ studied the relative importance of different ice-dynamical processes for glacial terminations. The onset of terminations is dominated by a decrease in SMB, which ~~induces~~causes a retreat of the ice sheet. ~~The~~We found that the Eurasian ice sheet ~~is more sensitive to higher~~needs lower CO_2 concentrations and/or insolation compared to North America~~, and will therefore retreat more often~~ in order to survive a climate optimum. Once the ice sheets have retreated significantly, proglacial lakes are created at the margin of the ice sheets. Our results show that these proglacial lakes can significantly accelerate the collapse of the North American and Eurasian ice sheets. ~~If these~~ If certain processes facilitated by the lakes are ~~not present,~~removed, the North America and Eurasia deglaciate at a reduced pace, and ~~often~~may remain partially ice-covered~~.~~ during interglacial periods.

The largest impact ~~of~~that proglacial lakes have on deglaciations is ~~caused by the~~that they facilitate low friction ~~of~~under floating ice. If the basal friction of shelves is the same as grounded ice, which removes the effect of PLISI and MISI, the Eurasian ice sheet ~~does not fully melt and an ice-dome persists in the Barents-Kara Sea throughout the interglacial. While the North American ice sheet does eventually disappear, removing the lakes delays this by a few millennia. This is in line with Hinck et al. (2022) and Quinquet et al. (2021), who suggested that PLISI has a large impact on the melt of the North American ice sheet. We find that this is mainly due to the elevation-temperature feedback, where the high flow velocities of shelves cause them to thin. The resulting lower surface elevations result in increased surface melt.~~

~~We~~only fully melts during interglacial periods rather than interstadials, and more ice can persist through some interglacial periods. The high ice velocities caused by the negligible sub-shelf friction creates large shelves with low surface elevations, which have high temperatures and surface melt. Though, this process is also sensitive to the basal friction. By lowering basal friction, ice thickness at glacial maxima is decreased and consequentially, surface temperatures and melt are increased. Therefore, a lower friction results into a faster deglaciation. This shows that modelling sediments and hydrology are important to simulate glacial cycles. Furthermore, we found that sub-shelf melting is only a secondary effect to the mass loss of the ice sheets. Applying a zero sub-shelf melt rate still results in a full deglaciation, although it may take ~~a few additional centuries to complete. Applying a more sophisticated sub-shelf melting scheme in the Baseline experiment, to simulate high melt rates near the grounding line (Rignot and Jacobs, 2002), may result in a more substantial impact from sub-shelf melting. Nevertheless, this smaller impact of sub-shelf melting is in line with both Hinck et al. (2022) and Quinquet et al. (2021). Additionally, since proglacial lakes consist of fresh water, it is doubtful whether such high melt rates, which at present are a result of salinity-driven overturning, should be expected at all~~an additional millennium to complete.

~~________~~ We have also investigated the effect of the GIA response time on consecutive glacial cycles and deglaciations.~~The size and shape of proglacial lakes follow from the interaction between GIA and ice thickness. Here we have used uniform GIA response times, but in reality, GIA varies spatially (e.g., Forte et al., 2010) and have large uncertainties.~~ If the GIA responds slower compared to our Baseline, the termination will be up to a millennium slower and the subsequent inception phase is delayed. Since the inception sites are typically also the last regions to deglaciate, the land can still be below

sea level at the onset of the next glacial period only if the bedrock rebound is too slow. We find that a GIA response that is substantially faster than the Baseline has a slower deglaciation. The and larger interglacial ice volumes as the North American and Eurasian ice sheet may not even fully deglaciate during some interglacial periods. This is because proglacial lakes are not created when the bedrock uplift is too fast. Additionally, surface melt is reduced as the bedrock uplift more efficiently compensates the thickness loss.

The importance of understanding marine ice-sheet dynamics and ice-sheet climate interactions when projecting the future mass loss of the Greenland and Antarctic ice sheets is well known. Ourthought to be very important. For Antarctica, the marine equivalent to PLISI, MISI may induce a run-away collapse of parts of West-Antarctica (e.g. Ritz et al., 2015). Though this is not a perfect analogy, as for example the high sensitivity of the Eurasian ice sheet towards temperature does not perfectly translate to future Western-Antarctic melt (van Aalderen et al., 2023). Greenland is currently mostly land terminating, but proglacial lakes are created during the retreat, which is already being observed (e.g., Carrivick and Quincey, 2014). These lakes may accelerate the retreat of the Greenland ice sheet (Carrivick et al., 2022). Therefore, our results underline the fact that these processes are just as relevant for understanding past ice-sheet evolution, so that reproducing this evolution can help constrain these processes in the context of current changes in Antarctica and Greenland.

Code availability: The source code for IMAU-ICE can be found at https://github.com/IMAU-paleo/IMAU-ICE. The version used in this study as well as the configuration files are available at Zenodo [DOI will be added upon acceptation]. Running simulations requires additional files for CO_2 (see Bereiter et al., 2015), climate (PMIP3 database: https://esgf-node.ipsl.upmc.fr/search/cmip5-ipsl/; last access 24 nov 2023), insolation (Laskar et al., 2004) and initial topography (ETOPO; Amante and Eakins, 2009; Bedmachine; https://nsidc.org/data/idbmg4/versions/1; last access 9 feb 2024). LGM land and ice masks were obtained from Abe-Ouchi et al. (2015). Till friction angle was obtained from Gowan et al. (2019) and Laske and Masters (1997). For more information, contact the corresponding author.

Data availability: The results are available in a 5 kyr (2D fields) and 100-year (scalar) output frequency at Zenodo [DOI will be added upon acceptation]. Additional 2D fields and higher output frequencies up to 1 kyr can be requested by contacting the corresponding author.

Author contributions. MS conducted the simulations and has written the manuscript. The set-up for the experiments was created by RW, CB and MS. CB provided model support. All authors have provided input to the manuscript and analysis of the results.

Competing interest. The authors declare that they have no conflict of interest.

Acknowledgements. M.D.W. Scherrenberg is supported by the Netherlands Earth System Science Centre (NESSC), which is financially supported by the Ministry of Education, Culture and Science (OCW) on grant no. 024.002.001. C.J. Berends is funded by PROTECT. This project has received funding from the European Union's Horizon 2020 research and innovation programme under grant agreement No 869304, PROTECT contribution number [will be assigned upon publication]. The Dutch Research Council (NWO) Exact and Natural Sciences supported the supercomputer facilities for the Dutch National Supercomputer Snellius. We would like to acknowledge the support of SurfSara Computing and Networking Services.

Appendix A: Basal sliding, friction and hydrology

In this study, we have used a Budd-type sliding law to simulate the sliding at the base of the ice sheets. To obtain the friction under the base of the ice sheet, we applied a parameterisation based on Martin et al. (2011). Table 2 list the units and corresponding values of constants named here.

The pore water pressure (ψ) is parameterized based on Martin et al. (2011). The pore water pressure scaling factor (λ) determines the saturation of the base and depends on the local (x, y indexes) bedrock height (b) and concurrent sea level (SL):

$$\lambda = 1 - \frac{b(x,y) - SL - b_{\psi,min}}{b_{\psi,max} - b_{\psi,min}}. \tag{1}$$

The pore water pressure scaling factor is limited between 1 (fully saturated) and 0 (fully unsaturated). Here, $b_{\psi,max}$ is the bedrock elevation with respect to sea level at which beds become fully unsaturated (1000 m), while $b_{\psi,max}$ is the elevation when beds become fully saturated (0 m). This pore water pressure scaling factor is used in combination with the overburden pressure to calculate the pore water pressure (ψ):

$$\psi = P_w \, \rho \, g \, H(x,y) \, \lambda. \tag{2}$$

Here, H represents the thickness of the ice. P_w is the pore water pressure scaling fraction. Here we have used 0.99, which yields a good LGM ice sheet volume and extent in combination with the prescribed till friction map. To determine the till friction angle (ϕ), we use different data-sets for North America and Eurasia. For North America we use a geology reconstruction from Gowan et al. (2019), which has full coverage of our ice domain and indicates were bedrock could more easily erode. The map from Gowan et al. (2019) has been specifically created for ice sheet modelling. For Eurasia we have created a till friction angle map based on sediment thicknesses from Laske and Masters (1997), where till friction angles are 10 degrees when sediment thicknesses exceed 100 meters, while for other regions a value of 30 degrees is used. In the High Friction simulations, till friction angles are 30 degrees in North America and Eurasia, while the Low Friction simulations has till friction angles of 10 degrees. For Greenland, which is not the focus of our experiments, we always use the same till friction angle map of 30 degrees for land at present-day and 10 degrees for ocean. The pore water pressure and till friction angle can then be used to calculate the till yield stress (τ):

$$\tau(x,y) = \tan\left(\frac{pi}{180}\right)\phi\,(\rho\,g\,H(x,y) - \psi) \hspace{4cm} (3)$$

To calculate the basal friction coefficient (β), we use the Budd type sliding law (Bueler and van Pelt, 2015):

$$\beta(x,y) = \tau(x,y)\frac{u^{(q-1)}}{u_0^q} \hspace{4cm} (4)$$

Here, u represents the ice velocity. The sliding term, is then used to calculate the basal sliding. The basal friction coefficient is multiplied by the grounded fraction, which is calculated based on Leguy et al. (2021). Therefore, regions that are fully floating (grounded fraction of 0) receive a negligible friction, the grounding line (grounded fraction between 0 and 1) receive reduced friction, and fully grounded ice receive the full friction (grounded fraction of 1). For the Rough Water simulation, the basal friction coefficient is always multiplied by 1 instead and therefore the friction treats all ice as if it were grounded.

Table 2: Constants describing till friction angle and basal hydrology

Symbol	Description	Units	Value
$b_{\psi,min}$	Elevation with fully saturated beds	m	0
$b_{\psi,max}$	Elevation with fully unsaturated beds	m	1000
ρ	Density of ice	kg/m^3	910
g	Gravitational acceleration	m/s^2	9.81
P_w	Pore water pressure scaling		0.99
q	Exponent in Budd type sliding law		0.3
u_0	Threshold velocity in Budd type sliding law	m/yr	100

Appendix B: Climate time-slice interpolation

To provide the ice-sheet model with transiently changing forcing using minimal computational resources, we interpolate between pre-calculated LGM and PI climate time-slices. To interpolate the time-slices we have used a matrix method. Our approach is based on Berends et al. (2018) and Scherrenberg et al. (2023) and uses different methods for temperature and precipitation.

To calculate the temperature forcing, we use a linear interpolation:

$$T(x,y,m) = w_T(x,y)\,T_{PI}(x,y,m) + \left(1 - w_T(x,y)\right)T_{LGM}(x,y,m). \hspace{3cm} (5)$$

Here, T is the temperature forcing in the ice sheet model. T_{PI} and T_{LGM} are the climate model temperatures for PI and the LGM respectively. w_T is the interpolation weight and depends on two processes: the external forcing (w_e) and an albedo feedback (w_a). w_T is capped between -0.25 and 1.25 to prevent too much extrapolation. For North America and Eurasia, w_T is calculated as following:

$$w_T(x,y) = \frac{w_e(x,y)+w_a(x,y)}{2} \quad . \tag{6}$$

620 In Greenland the albedo changes almost exclusively due to the change in ice-sheet extent. Our model does not include sea ice and the Greenland domain does not contain extensive tundra areas. Therefore, we apply a smaller contribution from albedo:

$$w_T(x,y) = \frac{3\,w_e(x,y)+w_a(x,y)}{4} \quad . \tag{7}$$

To calculate w_e we combine the effect of CO_2 (ppm; Bereiter et al., 2015) and insolation at 65°N ($Q_{65°N}$; W/m^2; Laskar et al.,

625 2004):

$$w_e = \frac{C-C_{LGM}}{C_{PI}-C_{LGM}} + \frac{Q_{65°N}-440\,W/m^2}{70\,W/m^2} \quad . \tag{8}$$

In this equation, C_{PI} and C_{LGM} are 190 and 280 ppm respectively. By including the summer (June, July, August) insolation at 65°N ($Q_{65°N}$), the climate can become colder or warmer even if the CO_2 concentration is constant (see Fig. 2).

To calculate w_a, which represents an albedo feedback, we calculate the annual absorbed insolation by the surface.
630 The absorbed insolation (I) depends on the monthly internally calculated surface albedo (α_s) and insolation at the top of the atmosphere (Q):

$$I(x,y) = \sum_{m=1}^{12} Q(x,y,m)\left(1 - \alpha_s(x,y,m)\right) \quad . \tag{9}$$

The albedo is calculated in the ice-sheet model using Eq. 24 (see appendix D). To calculate an interpolation weight for the absorbed insolation (w_i), we need to calculate reference fields for the LGM and PI. To calculate the albedo for the LGM time-
635 slice, we use land and ice masks from the ice sheet reconstruction by Abe-Ouchi et al. (2015), as these were also used in the climate model simulations. We integrate the SMB model forward through time with a fixed climate and ice-sheet geometry until the firn layer reaches a steady state (typically after ~30 years). We can then use Eq. 9 to calculate the reference fields for absorbed insolation. These absorbed insolation fields can then be used to calculate w_i.

$$w_i(x,y) = \left(I(x,y) - I_{LGM}(x,y)\right) / \left(I_{PI}(x,y) - I_{LGM}(x,y)\right) \quad . \tag{10}$$

640 To account for both the local and domain wide change in albedo and insolation, we use the following equation:

$$w_a(x,y) = \frac{w_i(x,y)+3\,w_{i,smooth}(x,y) + 3\,w_{i,domain}(x,y)}{7} \quad . \tag{11}$$

Here, $w_{i,domain}$ is the domain-wide averaged interpolation weight and w_i is the local interpolation weight. $w_{i,smooth}$ represents the regional temperature effect and is calculated by applying a 200 km gaussian smoothing on w_i. Once again, we use a different method for Greenland due to the lack of tundra regions:

645
$$w_a(x,y) = \frac{w_{i,smooth}(x,y) + 6\,w_{i,domain}}{7} \quad . \tag{12}$$

The interpolation weight to calculate temperature (w_T) can now be derived from w_a and w_e using Eq. 6 or 7. This interpolation weight will change depending on albedo, insolation and CO_2.

For precipitation, we apply a different method, as the precipitation does not change linearly when the climate cools down and topography changes. We use the following equation to interpolate the precipitation from the climate time-slices:

$$P = exp\big((1 - w_P(x,y))\log\big(P_{PI}(x,y,m)\big) + w_P(x,y)\log\big(P_{LGM}(x,y,m)\big)\big). \tag{13}$$

w_P is the interpolation weight and depends on local and domain-wide topography changes. First, we compare the domain-wide topography in the model to the climate time-slices using the following equation:

$$w_{s,domain} = \Big(\sum s(x,y) - \sum s_{PI}(x,y)\Big) / \Big(\sum s_{LGM}(x,y) - \sum s_{PI}(x,y)\Big). \tag{14}$$

The surface topography is represented by s. $w_{s,domain}$ represents the interpolation weight from the domain-wide change in topography. If a grid-cell was covered with ice during the LGM, we also interpolate with respect to local changes in topography:

$$w_{S,local}(x,y) = \frac{S(x,y) - S_{PI}(x,y)}{S_{LGM}(x,y) - S_{PI}(x,y)} \, w_s(x,y). \tag{15}$$

If a grid-cell did not have ice during the LGM, $w_{s,local}$ is equal to $w_{s,domain}$. In the last step, we multiply the local and regional precipitation effect to obtain the interpolation weight for precipitation:

$$w_P(x,y) = w_{S,local}(x,y) \, w_{S,domain}(x,y). \tag{16}$$

The resulting w_P from Eq. 16 is used in Eq. 13 to calculate the interpolated precipitation forcing.

Appendix C: Downscaling and bias correction

To account for differences between the general circulation model (GCM) simulations and observed climate (ERA40; Uppala et al., 2005), we apply a bias correction on both the LGM and PI snapshots.

To account for the temperature bias, we first have to scale the temperature to sea level using a lapse-rate correction. This is to account for differences in topography between the GCM and ERA40 data.

$$T_{obs,SL}(x,y,m) = T_{obs}(x,y,m) + s_{obs}(x,y)\,\lambda(x,y). \tag{17}$$

$$T_{GCM,SL}(x,y,m) = T_{GCM,PI}(x,y,m) + s_{GCM,PI}(x,y)\,\lambda(x,y). \tag{18}$$

Here, T is the temperature from ERA40 (obs) and the pre-industrial (PI) time-slices of the climate model (GCM). Surface height is defined as s. The temperature lapse rate (λ) is equal to 0.008 K/m. Once the temperature is applied to sea level (SL), we calculate the temperature difference between the climate model and observed climate:

$$T_{GCM,bias}(x,y,m) = T_{GCM,SL}(x,y,m) - T_{obs,SL}(x,y,m). \tag{19}$$

This bias correction is then subtracted from the PI and LGM snapshots. As a result, the PI snapshot will be the equal to ERA40, which contains some anthropogenic warming.

For precipitation (P), biases are applied as ratios rather than absolute differences, to ensure that the bias-corrected values are always positive. Therefore, we use the ratio between the model and observed fields instead:

$$P_{GCM,bias}(x,y,m) = P_{GCM}(x,y,m) / P_{obs}(x,y,m). \tag{20}$$

This ratio is used to calculate the bias corrected precipitation for PI and LGM:

$$P(x,y,m) = P_{GCM}(x,y,m) / P_{GCM,bias}(x,y,m). \tag{21}$$

Appendix D: Surface mass balance model

The surface mass balance (SMB) is calculated using an insolation-temperature model; IMAU-ITM (Berends et al., 2018). To calculate the SMB, ice is added due to snow and refreezing and is removed due to melt. To calculate accumulation and ablation of ice, the model requires temperature and precipitation fields, which were obtained from downscaled and bias-corrected GCM output (see appendix B and C). To calculate the amount of snowfall, we apply a temperature-based snow-rain partitioning with respect to the melting point ($T0$) by Ohmura et al. (1999).

$$f_{snow} = f = 0.5 \left(1 - \frac{atan\frac{(T(x,y,m)-T0)}{3.5}}{1.25664}\right)\left(1 - \frac{atan\frac{(T(x,y,m)-T_0)}{3.5}}{1.25664}\right). \tag{22}$$

The snow fraction (f_{snow} f) determines the amount of precipitation that falls as snow; the remainder falls as rain. The snow fraction is limited so it always is between 0 (100% rain) and 1 (100% snow). x and y indicate the horizontal grid while m indicates the month. To calculate the ablation of ice, we use the parameterised scheme by Bintanja et al. (2002) that accounts for ablation from temperature and insolation:

$$Melt\,M(x,y,m) = (c_1 \left(T(x,y,m) - T_0\right) + c_2 \left(1 - \alpha(x,y,m)\right) Q_{TOA}(x,y,m) Q(x,y,m) - c_3). \tag{23}$$

Here, T is the 2-meter air temperature, T_0 is the melting temperature of ice or 273.$\frac{15}{16}$ K, Q_{TOA} is the insolation at the top of the atmosphere (Laskar et al., 2004). The parameters for c_1, c_2 are 0.079 m/yr/K and 7.9×10^{-4} m/J/yr. The parameter c_3 is used for tuning. Here we have tuned the model to obtain realistic LGM ice volumes, with c_3 values for North America (-0.$\frac{28}{16}$ m/yr) Eurasia (-0.24 m/yr) and Greenland (0.19 m/yr). Albedo (α) is calculated in the ice-sheet model and is also based on Bintanja et al. (2002):

$$\alpha_{surface}(x,y,m)\,\alpha(x,y,m) = \alpha_{snow} - (\alpha_{snow} - \alpha_{background})e^{-15\,D_{firn}(x,y,m-1)}(\alpha_{snow} - \alpha_b)\exp^{-15m^{-1}\,D(x,y,m-1)} -$$
$$0.015\,Melt_{prev}\,m^{-1}M_{prev}(x,y). \tag{24}$$

The $\alpha_{background}$ α_b represents the albedo without any snow, with 0.5 for bare ice, 0.2 for land and 0.1 for water. Melt of the previous year is defined as $Melt_{prev}$. If snow is added on top, which increases the firn depth (D_{firn}, D), the albedo can increase until α_{snow}, which represents the albedo of fresh snow (0.85). Therefore, the albedo in the model varies between the background and snow albedo. The depth of the firn layer is calculated using the amount of snow that is added on top without melting.

Some of the melt and rainfall can refreeze in the model. Here we use the approach by Huybrechts and de Wolde (1999), using the total amount of liquid water (L l), superimposed water (S s) and precipitation (P).

$$Ss(x,y,m) = max\{0,0.012(T0 - T(x,y,m))\}\,max\{0, 0.012\,m/yr\left(T_0 - T(x,y,m)\right)\}. \tag{25}$$

$$Ll(x,y,m) = Rain\,R(x,y,m) + Melt\,M(x,y,m). \tag{26}$$

$$Refreezing\,r(x,y,m) = min\{min\{S(x,y,m), L(x,y,m)\}, P(x,y,m)\}. \tag{27}$$

By combining the snowfall, refreezing and melt the SMB can be calculated:

$$SMB(x, y, m) = SnowS(x, y, m) + Refreezingr(x, y, m) - MeltM(x, y, m). \tag{7 (28)}$$

Appendix B: Downscaling and bias correction

715 To account for differences between the general circulation model (GCM) simulations and observed climate (ERA40; Uppala et al., 2005), we apply a bias correction on both the LGM and PI snapshots.

To account for the temperature bias, we first have to scale the temperature to sea level using a lapse-rate correction. This is to account for differences in topography between the GCM and ERA40 data.

$$T_{obs,SL}(x, y, m) = T_{obs,PD}(x, y, m) + Hs_{obs,PD}(x, y) \lambda(x, y). \tag{8}$$

720
$$T_{GCM,SL}(x, y, m) = T_{GCM,PI}(x, y, m) + Hs_{GCM,PI}(x, y) \lambda(x, y). \tag{9}$$

Here, T is the temperature from ERA40 (obs) and the climate model (GCM). Surface height is defined as Hs_{GCM}. The temperature lapse rate is represented by λ. Once the temperature is applied to sea level (SL), we calculate the temperature difference between the climate model and observed climate:

$$T_{GCM,BIAS}(x, y, m) = T_{GCM,SL}(x, y, m) - T_{obs,SL}(x, y, m). \tag{10}$$

725 This bias correction is then subtracted from the PI and LGM snapshots. As a result, the PI snapshot will be the equal to ERA40, which contains some anthropogenic warming.

For precipitation, biases are applied as ratios rather than absolute differences, to ensure that the bias-corrected values are always positive. Therefore, we use the ratio between the model and observed fields instead:

$$P_{GCM,BIAS}(x, y, m) = P_{GCM,PI}(x, y, m) / P_{obs,PI}(x, y, m). \tag{11}$$

730 This ratio is used to calculate the bias corrected precipitation for PI and LGM:

$$P_{GCM,corr}(x, y, m) = P_{GCM}(x, y, m) / P_{GCM,bias}(x, y, m). \tag{12}$$

Appendix C: Climate time-slice interpolation

To provide the ice-sheet model with transiently changing forcing using minimal computational resources, we interpolate between pre-calculated LGM and PI climate time-slices. To interpolate the time-slices we have used a matrix method. Our

735 approach is based on Berends et al. (2018) and Scherrenberg et al. (2023) and uses different methods for temperature and precipitation.

To calculate the temperature forcing, we use a linear interpolation:

$$T_{mod}(x, y, m) = w_{tot,T}(x, y) T_{PI,corr}(x, y, m) + \left(1 - w_{tot,T}(x, y)\right) T_{LGM,corr}(x, y, m). \tag{13}$$

Here, T_{mod} is the temperature forcing in the ice sheet model. $T_{PI,corr}$ and $T_{LGM,corr}$ are the climate model temperatures for PI and LGM respectively. w_{tot} is the interpolation weight and depends on two processes: the external forcing (w_{ext}) and an albedo feedback (w_{ice}). For North America and Eurasia, w_{tot} is calculated as following:

$$w_{tot,T}(x,y) = \frac{(w_{ext}(x,y) + w_{ice}(x,y))}{2} . \tag{14}$$

In Greenland the albedo changes almost exclusively due to the change in ice-sheet extent. Our model does not include sea ice and the Greenland domain does not contain extensive tundra areas. Therefore, we apply a smaller contribution from albedo in this domain:

$$w_{tot,T}(x,y) = \frac{(3\, w_{ext}(x,y) + w_{ice}(x,y))}{4} . \tag{15}$$

To calculate w_{ext} we combine the effect of CO_2 (ppm; Bereiter et al., 2015) and insolation at 65°N (W/m^2; Laskar et al., 2004):

$$w_{ext} = \frac{CO2 - CO2_{LGM}}{CO2_{PI} - CO2_{LGM}} + \frac{QTOA_{65°N} - 440}{70} . \tag{16}$$

In this equation, $CO2_{PI}$ and $CO2_{LGM}$ are 190 and 280 ppm respectively. By including the summer (June, July, August) insolation at 65°N ($QTOA_{65°N}$), the climate can become colder or warmer even if the CO_2 concentration is constant (see Fig. 1).

To calculate w_{ice}, which represents an albedo feedback, we calculate the annual absorbed insolation. The absorbed insolation (I_{abs}) depends on the monthly internally calculated albedo ($\alpha_{surface}$) and insolation at the top of the atmosphere (Q_{TOA}):

$$I_{abs}(x,y) = \sum_{m=1}^{12} Q_{TOA}(x,y,m) \left(1 - \alpha_{surface}(x,y,m)\right) . \tag{17}$$

The albedo is calculated in the ice-sheet model using Eq. 3. To calculate an interpolation weight, from the absorbed insolation (w_{ins}), we need to calculate reference fields for the LGM and PI. To calculate the albedo for these time slices, we use land and ice masks from the ice sheet reconstruction by Abe-Ouchi et al. (2015) as these were also used in the climate model simulations. We integrate the SMB model forward through time with a fixed climate and ice-sheet geometry until the firn layer reaches a steady state (typically after ~30 years). We can then use Eq. 17 to calculate the reference fields for absorbed insolation. These absorbed insolation fields can then be used to calculate w_{ins}.

$$w_{ins}(x,y) = (I_{abs}(x,y) - I_{abs,LGM}(x,y)) / (I_{abs,PI}(x,y) - I_{abs,LGM}(x,y)) . \tag{18}$$

To account for both the local and domain wide change in albedo and insolation, we use the following equation:

$$w_{ice}(x,y) = \frac{w_{ins}(x,y) + 3\, w_{ins,smooth}(x,y) + 3\, w_{ins,av}(x,y)}{7} . \tag{19}$$

Here, $w_{ins,av}$ is the domain-wide averaged interpolation weight and w_{ins} is the local interpolation weight. $w_{ins,smooth}$ represents the regional temperature effect and is calculated by applying a 200 km gaussian smoothing on w_{ins}. Once again, we use a slightly different method for Greenland due to the lack of tundra regions:

$$w_{ice}(x,y) = \frac{w_{ins,smooth}(x,y) + 6\, w_{ins,av}}{7} . \tag{20}$$

The interpolation weight to calculate temperature ($w_{tot,T}$) can now be derived from w_{ice} and w_{ext} using Eq. 14 or 15. This interpolation weight will change depending on albedo, insolation and CO_2.

For precipitation, we apply a slightly different method, as the precipitation does not change linearly when the climate cools down and topography changes. We use the following equation to interpolate the precipitation from the climate time slices:

$$P_{ref} = e\left((1 - w_{LGM}(x,y))\log\left(P_{PI,corr}(x,y,m)\right) + w_{LGM}(x,y)\log\left(P_{LGM,corr}(x,y,m)\right)\right). \tag{21}$$

w_{LGM} is the interpolation weight and depends on local and domain-wide topography changes. First, we compare the domain-wide topography in the model to the climate time slices using the following equation:

$$w_{tot,P} = \left(\sum Hs(x,y) - \sum Hs_{PI}(x,y)\right) / \left(\sum Hs_{LGM}(x,y) - \sum Hs_{PI}(x,y)\right). \tag{22}$$

The surface topography is represented by Hs. $w_{tot,P}$ represents the interpolation weight from the domain-wide change in topography. If a grid-cell was covered with ice during the LGM, we also interpolate with respect to local changes in topography:

$$w_{LGM,Hs}(x,y) = \frac{Hs_{ISM}(x,y) - Hs_{GCM,PI}(x,y)}{Hs_{GCM,LGM}(x,y) - Hs_{GCM,PI}(x,y)} w_{tot,P}(x,y). \tag{23}$$

If a grid-cell did not have ice during the LGM, $w_{LGM,Hs}$ is equal to $w_{tot,P}$. In the last step, we multiply the local and regional precipitation effect to obtain the interpolation weight for precipitation:

$$w_{LGM}(x,y) = w_{LGM,Hs}(x,y)\, w_{tot,P}(x,y). \tag{24}$$

The resulting w_{LGM} from Eq. 24 is used in Eq. 20 to calculate the precipitation forcing.

Code availability: The source code for IMAU ICE can be found at https://github.com/IMAU-paleo/IMAU-ICE. The version used in this study as well as the configuration files are available at Zenodo [DOI will be added upon acceptation]. To run the simulations additional files are required for CO_2, climate and initial topography. For more information, contact the corresponding author.

Data availability: The results are available in a 5 kyr (2D fields) and 100-year (scalar) output frequency at Zenodo [DOI will be added upon acceptation]. Additional 2D fields and higher output frequencies up to 1 kyr can be requested by contacting the corresponding author.

Author contributions. MS conducted the simulations and has written the manuscript. The set-up for the experiments was created by RW, CB and MS. CB provided model support. All authors have provided input to the manuscript and analysis of the results.

Competing interest. The authors declare that they have no conflict of interest

Acknowledgements. ~~M.D.W. Scherrenberg is supported by the Netherlands Earth System Science Centre (NESSC), which is financially supported by the Ministry of Education, Culture and Science (OCW) on grant no. 024.002.001. C.J. Berends is funded by PROTECT. This project has received funding from the European Union's Horizon 2020 research and innovation programme under grant agreement No 869304, PROTECT contribution number [will be assigned upon publication]. The Dutch Research Council (NWO) Exact and Natural Sciences supported the supercomputer facilities for the Dutch National Supercomputer Snellius. We would like to acknowledge the support of SurfSara Computing and Networking Services.~~

References

Abe-Ouchi, A., Saito, F., Kawamura, K., Raymo, M. E., Okuno, J., Takahashi, K., and Blatter, H.: Insolation-driven 100,000-year glacial cycles and hysteresis of ice-sheet volume, Nature, 500, 190–193, https://doi.org/10.1038/nature12374, 2013.

Abe-Ouchi, A., Saito, F., Kageyama, M., Braconnot, P., Harrison, S. P., Lambeck, K., Otto-Bliesner, B. L., Peltier, W. R., Tarasov, L., Peterschmitt, J.-Y., and Takahashi, K.: Ice-sheet configuration in the CMIP5/PMIP3 Last Glacial Maximum experiments, Geosci. Model Dev., 8, 3621–3637, https://doi.org/10.5194/gmd-8-3621- 2015, 2015.

Alder, J. R. and Hostetler, S. W.: Applying the Community Ice Sheet Model to evaluate PMIP3 LGM climatologies over the North American ice sheets, Clim. Dynam., 53, 2807–2824, https://doi.org/10.1007/s00382-019-04663-x, 2019.

Annan, J. D., Hargreaves, J. C., and Mauritsen, T.: A new global surface temperature reconstruction for the Last Glacial Maximum, Clim. Past, 18, 1883–1896, ~~https://doi.org/10.5194/cp-18-1883-2022,~~ https://doi.org/10.5194/cp-18-1883-2022, 2022

Austermann, J., Wickert, A. D., Pico, T., Kingslake, J., Callaghan, K. L., and Creel, R. C.: Glacial isostatic adjustment shapes proglacial lakes over glacial cycles, Geophys. Res. Lett., 50, e2022GL101191. https://doi.org/10.1029/2022GL101191, 2022

Batchelor, C. L., Margold, M., Krapp, M., Murton, D., Dalton, A. S., Gibbard, P. L., Stokes, C. R., Murton, J. B., and Manica, A.: The configuration of Northern Hemisphere ice sheets through the Quaternary, Nat. Commun., 10, 3713, https://doi.org/10.1038/s41467-019-11601-2, 2019.

Beghin, P., Charbit, S., Dumas, C., Kageyama, M., and Ritz, C.: How might the North American ice sheet influence the northwestern Eurasian climate?, Clim. Past, 11, 1467–1490, https://doi.org/10.5194/cp-11-1467-2015, 2015.

Benn, D. I., Warren, C. R., and Mottram, R. H.: Calving processes and the dynamics of calving glaciers, Earth-Sci. Rev., 82, 143– 179, https://doi.org/10.1016/J.EARSCIREV.2007.02.002, 2007.

Bereiter, B., Eggleston, S., Schmitt, J., Nehrbass-Ahles, C., Stocker, T. F., Fischer, H., Kipfstuhl, S., and Chappellaz, J.: Revision of the EPICA Dome C CO2 record from 800 to 600kyr before present, Geophys. Res. Lett., 42, 542–549, https://doi.org/10.1002/2014GL061957, 2015.

Berends, C. J. and van de Wal, R. S. W.: A computationally efficient depression-filling algorithm for digital elevation models, applied to proglacial lake drainage, Geosci. Model Dev., 9, 4451–4460, https://doi.org/10.5194/gmd-9-4451-2016, 2016.

Berends, C. J., de Boer, B., and van de Wal, R. S. W.: Application of HadCM3@Bristolv1.0 simulations of paleoclimate as

835   forcing for an ice-sheet model, ANICE2.1: set-up and benchmark experiments, Geosci. Model Dev., 11, 4657–4675, https://doi.org/10.5194/gmd-11-4657-2018, 2018.

Berends, C. J., Köhler, P., Lourens, L. J., and van de Wal, R. S. W.: On the cause of the mid-Pleistocene transition, Rev. Geophys., 59, e2020RG000727, https://doi.org/10.1029/2020RG000727, 2021.

Berends, C. J., Goelzer, H., Reerink, T. J., Stap, L. B., and van de Wal, R. S. W.: Benchmarking the vertically integrated ice-

840   sheet model IMAU-ICE (version 2.0), Geosci. Model Dev., 15, 5667–5688, https://doi.org/10.5194/gmd-15-5667-2022, 2022.

Bintanja, R., van de Wal, R. S. W., and Oerlemans, J.: Global ice volume variations through the last glacial cycle simulated by a 3-D ice dynamical model, Quatern. Int., 95–96, 11–23, 2002.

Bonelli, S., Charbit, S., Kageyama, M., Woillez, M.-N., Ramstein, G., Dumas, C., and Quiquet, A.: Investigating the evolution

845   of major Northern Hemisphere ice sheets during the last glacial-interglacial cycle, Clim. Past, 5, 329–345, https://doi.org/10.5194/cp-5-329-2009, 2009.

Braconnot, P., Harrison, S. P., Otto-Bliesner, B. L., Abe-Ouchi, A., Jungclaus, J. H., and Peterschmitt, J.-Y.: The Paleoclimate Modeling Intercomparison Project contribution to CMIP5, CLIVAR Exchanges, 56, 15–19, 2011.

Budich, R., Gioretta, M., Jungclaus, J., Redler, R., and Reick, C.: The MPI-M Millennium Earth System Model: An assembling

850   guide for the COSMOS configuration, Tech. rep., Max-Planck Institute for Meteorology, Hamburg, Germany, https://pure.mpg. de/rest/items/item_2193290/component/file_2193291/content (last access: 2 February 2023), 2010.

Bueler, E. and Brown, J.: The shallow shelf approximation as a sliding law in a thermomechanically coupled ice sheet model, J. Geophys. Res., 114, F03008, https://doi.org/10.1029/2008JF001179, 2009.

Bueler, E. and van Pelt, W.: Mass-conserving subglacial hydrology in the Parallel Ice Sheet Model version 0.6, Geosci. Model

855   Dev., 8, 1613–1635, https://doi.org/10.5194/gmd-8-1613-2015, 2015.

Carrivick, J. L. and Quincey, D. J.: Progressive increase in number and volume of ice-marginal lakes on the western margin of the Greenland Ice Sheet, Global Planet. Change, 116, 156–163, https://doi.org/10.1016/j.gloplacha.2014.02.009, 2014.

Carrivick, J. L., How, P., Lea, J. M., Sutherland, J. L., Grimes, M., Tweed, F. S., Cornford, S., Quincey, D. J., and Mallalieu, J.: Ice-Marginal Proglacial Lakes Across Greenland: Present Status and a Possible Future, Geophys. Res. Lett., 49,

860   e2022GL099276, https://doi.org/10.1029/2022GL099276, 2022.

Charbit, S., Ritz, C., Philippon, G., Peyaud, V., and Kageyama, M.: Numerical reconstructions of the Northern Hemisphere ice sheets through the last glacial-interglacial cycle, Clim. Past, 3, 15–37, https://doi.org/10.5194/cp-3-15-2007, 2007.

Clark, P. and Pollard, D.: Origin of the Middle Pleistocene Transition by ice sheet erosion of regolith, Paleoceanography, 13, 1–9, https://doi.org/10.1029/97PA02660, 1998.

865 Clark, P. U. and Tarasov, L.: Closing the sea level budget at the Last Glacial Maximum, P. Natl. Acad. Sci., 111, 15861–15862, https://doi.org/10.1073/pnas.1418970111, 2014.

Claussen, M., Ganopolski, A., Brovkin, V., Gerstengarbe, F.-W., and, Werner, P.: Simulated global-scale response of the climate system to Dansgaard/Oeschger and Heinrich events, Clim. Dynam., 21, 361–370, https://doi.org/10.1007/s00382-003-0336-2, 2003.

870 Condron, A. and Winsor, P.: Meltwater routing and the Younger Dryas, P. Natl. Acad. Sci., 109, 19928–19933, doi:10.1073/pnas.1207381109, 2012.

Cutler, P. M., Mickelson, D. M., Colgan, P. M., MacAyeal, D. R., and Parizek, B. R.: Influence of the Great Lakes on the Dynamics of the Southern Laurentide Ice Sheet: Numerical Experiments, Geology, 29, 1039–1042, https://doi.org/10.1130/0091-7613(2001)029<1039:IOTGLO>2.0.CO;2, 2001.

875 Dalton, A. S., Margold, M., Stokes, C. R., Tarasov, L., Dyke, A. S., Adams, R. S., Allard, S., Arends, H. E., Atkinson, N., Attig, J. W., Barnett, P. J., Barnett, R. L., Batterson, M., Bernatchez, P., Borns, H. W., Breckenridge, A., Briner, J. P., Brouard, E., Campbell, J. E., Carlson, A. E., Clague, J. J., Curry, B. B., Daigneault, R. A., Dubé-Loubert, H., Easterbrook, D. J., Franzi, D. A., Friedrich, H. G., Funder, S., Gauthier, M. S., Gowan, A. S., Harris, K. L., Hétu, B., Hooyer, T. S., Jennings, C. E., Johnson, M. D., Kehew, A. E., Kelley, S. E., Kerr, D., King, E. L., Kjeldsen, K. K., Knaeble, A. R., 880 Lajeunesse, P., Lakeman, T. R., Lamothe, M., Larson, P., Lavoie, M., Loope, H. M., Lowell, T. V., Lusardi, B. A., Manz, L., McMartin, I., Nixon, F. C., Occhietti, S., Parkhill, M. A., Piper, D. J., Pronk, A. G., Richard, P. J., Ridge, J. C., Ross, M., Roy, M., Seaman, A., Shaw, J., Stea, R. R., Teller, J. T., Thompson, W. B., Thorleifson, L. H., Utting, D. J., Veillette, J. J., Ward, B. C., Weddle, T. K. and Wright, H. E.: An updated radiocarbon-based ice margin chronology for the last deglaciation of the North American Ice Sheet Complex, Quaternary Sci. Rev., 234, 106223, 885 https://doi.org/10.1016/j.quascirev.2020.106223, 2020.

de Boer, B., van de Wal, R., Lourens, L. J., Bintanja, R., and Reerink, T. J.: A continuous simulation of global ice volume over the past 1 million years with 3-D ice-sheet models, Clim. Dynam., 41, 1365–1384, 2013.

Denton, G. H., Anderson, R. F., Toggweiler, J., Edwards, R., Schaefer, J., and Putnam, A.: The last glacial termination, Science, 328, 1652–1656, https://doi.org/10.1126/science.1184119, 2010. Dufresne, J.-L., Foujols, M.-A., Denvil, S., 890 Caubel, A., Marti, O., Aumont, O., Balkanski, Y., Bekki, S., Bellenger, H., Benshila, R., Bony, S., Bopp, L., Braconnot, P., Brockmann, P., Cadule, P., Cheruy, F., Codron, F. F., Cozic, A., Cugnet, D., de Noblet, N., Duvel, J.-P., Ethé, C., Fairhead, L., Fichefet, T., Flavoni, S., Friedlingstein, P., Grandpeix, J.-Y., Guez, L., Guilyardi, E., Hauglustaine, D., Hourdin, F., Idelkadi, A., Ghattas, J., Joussaume, S., Kageyama, M., Krinner, G., Labetoulle, S., Lahellec, A., Lefèvre, M.-P., Lefèvre, F., Lévy, C., Li, Z. X., Lloyd, J., Lott, F., Madec, G., Mancip, M., Marchand, M., Masson, S., Meurdesoif, Y., Mignot, J., 895 Musat, I., Parouty, S., Polcher, J., Rio, C., Schulz, M., Swingedouw, D., Szopa, S., Talandier, C., Terray, P., and Viovy, N.: Climate change projections using the IPSL-CM5 Earth System Model: from CMIP3 to CMIP5, Clim. Dynam., 40, 2123–2165, https://doi.org/10.1007/s00382-012-1636-1, 2013.

Dufresne, J.-L., Foujols, M.-A., Denvil, S., Caubel, A., Marti, O., Aumont, O., Balkanski, Y., Bekki, S., Bellenger, H., Benshila, R., Bony, S., Bopp, L., Braconnot, P., Brockmann, P., Cadule, P., Cheruy, F., Codron, F. F., Cozic, A., Cugnet, D., de Noblet, N., Duvel, J.-P., Ethé, C., Fairhead, L., Fichefet, T., Flavoni, S., Friedlingstein, P., Grandpeix, J.-Y., Guez, L., Guilyardi, E., Hauglustaine, D., Hourdin, F., Idelkadi, A., Ghattas, J., Joussaume, S., Kageyama, M., Krinner, G., Labetoulle, S., Lahellec, A., Lefèbvre, M.-P., Lefèvre, F., Lévy, C., Li, Z. X., Lloyd, J., Lott, F., Madec, G., Mancip, M., Marchand, M., Masson, S., Meurdesoif, Y., Mignot, J., Musat, I., Parouty, S., Polcher, J., Rio, C., Schulz, M., Swingedouw, D., Szopa, S., Talandier, C., Terray, P., and Viovy, N.: Climate change projections using the IPSL-CM5 Earth System Model: from CMIP3 to CMIP5, Clim. Dynam., 40, 2123–2165, https://doi.org/10.1007/s00382-012-1636-1, 2013.

Feldmann, J., Albrecht, T., Khroulev, C., Pattyn, F., and Levermann, A.: Resolution-dependent performance of grounding line motion in a shallow model compared with a full-Stokes model according to the MISMIP3d intercomparison, J. Glaciol., 60, 353–359, https://doi.org/10.3189/2014JoG13J093, 2014.

Fettweis, X., Hofer, S., Krebs-Kanzow, U., Amory, C., Aoki, T., Berends, C. J., Born, A., Box, J. E., Delhasse, A., Fujita, K., Gierz, P., Goelzer, H., Hanna, E., Hashimoto, A., Huybrechts, P., Kapsch, M.-L., King, M. D., Kittel, C., Lang, C., Langen, P. L., Lenaerts, J. T. M., Liston, G. E., Lohmann, G., Mernild, S. H., Mikolajewicz, U., Modali, K., Mottram, R. H., Niwano, M., Noël, B. P. Y., Ryan, J. C., Smith, A., Streffing, J., Tedesco, M., van de Berg, W. J., van den Broeke, M. R., van de Wal, R. S. W., van Kampenhout, L., Wilton, D., Wouters, B., Ziemen, F., and Zolles, T.: GrSMBMIP: intercomparison of the modelled 1980-2012 surface mass balance over the Greenland Ice Sheet, The Cryosphere 14, 3935-3958, https://doi.org/10.5194/tc-14-3935-2020, 2020.

Flowers, G. E.: Modelling water flow under glaciers and ice sheets, P. Roy. Soc. A-Math. Phy., 471, 20140907, https://doi.org/10.1098/rspa.2014.0907, 2015.

Forte, A., Moucha, R., Simmons, N. A., Grand, S. P., and Mitro viceMitrovica, J. X.: Deep-mantle contributions to the surface dynamics of the North American continent, Tectonophysics, 481, 3–15, https://doi.org/10.1016/j.tecto.2009.06.010, 2010.

Ganopolski, A. and Calov, R.: The role of orbital forcing, carbon dioxide and regolith in 100 kyr glacial cycles, Clim. Past, 7, 1415–1425, https://doi.org/10.5194/cp-7-1415-2011, 2011.

Geirsdóttir, Á., Miller, G. H., Wattrus, N. J., Björnsson, H., and Thors, K.: Stabilization of glaciers terminating in closed water bodies: Evidence and broader implications, Geophys. Res. Lett, 35, L17502, https://doi.org/10.1029/2008GL034432, 2008.

Gomez, N., Weber, M. E., Clark, P. U., Mitrovica, J. X., and Han, H. K.: Antarctic ice dynamics amplified by Northern Hemisphere sea-level forcing, Nature, 587, 600–604, https://doi.org/10.1038/s41586-020-2916-2, 2020.

Gowan, E. J., Niu, L., Knorr, G., and Lohmann, G.: Geology datasets in North America, Greenland and surrounding areas for use with ice sheet models, Earth Syst. Sci. Data, 11, 375–391, https://doi.org/10.5194/essd-11-375-2019, 2019.

Gowan, E. J., Zhang, X., Khosravi, S., Rovere, A., Stocchi, P., Hughes, A. L. C., Gyllencreutz, R., Mangerud, J., Svendsen, J.- 655 I., and Lohmann, G.: A new global ice sheet reconstruction for the past 80 000 years, Nature Communications, 12, 1199, https://doi.org/10.1038/s41467-021-21469-w, 2021.

Grant, K. M., Rohling, E. J., Bronk Ramsey, C., Cheng, H., Edwards, R. L., Florindo, F., Heslop, D., Marra, F., Roberts, A. P., Tamisiea, M. E., and Williams, F.: Sea-level variability over five glacial cycles, Nature Communications, 5, 5076, https://doi.org/10.1038/ncomms6076, 2014.

Hasenfratz, A. P., Jaccard, S. L., Martínez-García, A., Sigman, D. M., Hodell, D. A., Vance, D., Bernasconi, S. M., Kleiven, H. F., Haumann, F. A., and Haug, G. H.: The residence time of Southern Ocean surface waters and the 100 000-year ice age cycle, Science, 363, 1080–1084, https://doi.org/10.1126/science.aat7067, 2019.

Hearty, P. J., Kindler, P., Cheng, H., and Edwards, R. L.: A +20 m middle Pleistocene sea-level highstand (Bermuda and the Bahamas) due to partial collapse of Antarctic ice, Geology, 27, 375–378, https://doi.org/10.1130/0091-7613(1999)027<0375:AMMPSL>2.3.CO;2, 1999.

Hildes, D. H., Clarke, G. K., Flowers, G. E., and Marshall, S. J.: Subglacial erosion and englacial sediment transport modelled for North American ice sheets, Quaternary Sci. Rev., 23, 409–430, https://doi.org/10.1016/j.quascirev.2003.06.005, 2004

Hinck, S., Gowan, E. J., Zhang, X., and Lohmann, G.: PISM-LakeCC: Implementing an adaptive proglacial lake boundary in an ice sheet model, The Cryosphere, 16, 941–965, https://doi.org/10.5194/tc-16-941-2022, 2022.

Hoffman, M. J. and Price, S.: Feedbacks between coupled sub-glacial hydrology and glacier dynamics, J. Geophys. Res.-Earth, 119, 414–436, https://doi.org/10.1002/2013JF002943, 2014.

Hughes, A. L. C., Gyllencreutz, R., Lohne, Ø. S., Mangerud, J., and Svendsen, J. I.: The last Eurasian ice sheets – a chronological database and time-slice reconstruction, DATED-1, Boreas, 45, 1–45, https://doi.org/10.1111/bor.12142, 2015.

Huybrechts, P. and de Wolde, J.: The dynamic response of the Greenland and Antarctic ice sheets to multiple-century climatic warming, J. Climate, 1, 2169–2188, 1999.

Janssens, I. and Huybrechts, P.: The treatment of meltwater retention in mass-balance parameterizations of the Greenland ice sheet, in: Ann. Glaciol., 31, 2000, edited by: Steffen, K., Ann. Glaciol., Int Glaciological Soc, Cambridge, 133–140, 2000.

Jungclaus, J., Giorgetta, M., Reick, C., Legutke, S., Brovkin, V., Crueger, T., Esch, M., Fieg, K., Fischer, N., Glushak, K., Gayler, V., Haak, H., Hollweg, H.-D., Kinne, S., Kornblueh, L., Matei, D., Mauritsen, T., Mikolajewicz, U., Müller, W., Notz, D., Pohlmann, T., Raddatz, T., Rast, S., Roeckner, E., Salzmann, M., Schmidt, H., Schnur, R., Segschneider, J., Six, K., Stockhause, M., Wegner, J., Widmann, H., Wieners, K.-H., Claussen, M., Marotzke, J., and Stevens, B.: CMIP5 simulations of the Max Planck Institute for Meteorology (MPI-M) based on the MPI- ESM-P model: The lgm experiment, served by ESGF, WDCC at DKRZ, https://doi.org/10.1594/WDCC/CMIP5.MXEPlg, 2012.

Ladant, J.-B., Donnadieu, Y., Lefebvre, V., and Dumas, C.: The respective role of atmospheric carbon dioxide and orbital parameters on ice sheet evolution at the Eocene Oligocene transition, Paleoceanography, 29, 810–823, https://doi.org/10.1002/2013PA002593, 2014.

Lambeck, K., Rouby, H., Purcell, A., Sun, Y., and Sambridge, M.: Sea level and global ice volumes from the Last Glacial Maximum to the Holocene, P. Natl. Acad. Sci. USA, 111, 15296–15303, https://doi.org/10.1073/pnas.1411762111, 2014.

Laskar, J., Robutel, P., Joutel, F., Gastineau, M., Correia, A. C. M., and Levrard, B.: A long-term numerical solution for the insolation quantities of the Earth, Astron. Astrophys., 428, 261–285, https://doi.org/10.1051/0004-6361:20041335, 2004.

965 Laske, G. and Masters, G.: A Global Digital Map of Sediment Thickness, EOS T. Am. Geophys. Un., 78, F483, 1997.

Leguy, G. R., Lipscomb, W. H., and Asay-Davis, X. S.: Marine ice sheet experiments with the Community Ice Sheet Model, The Cryosphere, 15, 3229–3253, https://doi.org/10.5194/tc-15-3229- 2021, 2021.

LeMeurLe Meur, E. and Huybrechts, P.: A comparison of different ways of dealing with isostasy: examples from modeling the Antarctic ice sheet during the last glacial cycle, Ann. Glaciol., 23, 309–
970 317, https://doi.org/10.3189/S0260305500013586, 1996.

Lepper, K., Buell, A. W., Fisher, T. G., and Lowell, T. V.: A chronology for glacial Lake Agassiz shorelines along Upham's namesake transect, Quaternary Res., 80, 88–98, https://doi.org/10.1016/j.yqres.2013.02.002, 2013.

Liakka, J., Löfverström, M., and Colleoni, F.: The impact of the North American glacial topography on the evolution of the Eurasian ice sheet over the last glacial cycle, Clim. Past, 12, 1225–1241, https://doi.org/10.5194/cp-12-1225-2016, 2016.

975 Löfverström, M., Caballero, R., Nilsson, J., and Messori, G.: Stationary Wave Reflection as a Mechanism for Zonalizing the Atlantic Winter Jet at the LGM, J. Atmos. Sci., 73, 3329–3342, https://doi.org/10.1175/JAS-D-15-0295.1, 2016.

Löfverström, M., Thompson, D. M., Otto-Bliesner, B. L., and Brady, E. C.: The importance of Canadian Arctic Archipelago gateways for glacial expansion in Scandinavia, Nat. Geosci, 15, 482-488, https://doi.org/10.1038/s41561-022-00956-9, 2022.

980 Mangerud, J., Alexanderson, H., Birks, H. H., Paus, A., Períc, Z. M., Svendsen, J. I.: Did the Eurasian ice sheets melt completely in early Marine Isotope Stage 3? New evidence from Norway and a synthesis for Eurasia, Quaternary Sci. Rev., 317, 108274, https://doi.org/10.1016/j.quascirev.2023.108136, 2023.

Martin, M. A., Winkelmann, R., Haseloff, M., Albrecht, T., Bueler, E., Khroulev, C., and Levermann, A.: The Potsdam Parallel Ice Sheet Model (PISM-PIK) – Part 2: Dynamic equilibrium simulation of the Antarctic ice sheet, The Cryosphere, 5, 727–
985 740, https://doi.org/10.5194/tc-5-727-2011, 2011.

McManus, J. F., Francois, R., Gherardi, J. M., Keigwin, L. D., and Brown-Leger, S.: Collapse and rapid resumption of Atlantic meridional circulation linked to deglacial climate changes, Nature, 428, 834–837, https://doi.org/10.1038/nature02494, 2004.

Melanson, A., Bell, T., and Tarasov, L.: Numerical modelling of subglacial erosion and sediment transport and its application to the North American ice sheets over the Last Glacial cycle, Quaternary Sci. Rev., 68, 154–174,
990 https://doi.org/10.1016/j.quascirev.2013.02.017, 2013.

Menviel, L. (2019). The southern amplifier. Science, 363, 1040–1041. https://doi.org/10.1126/science.aaw7196

Milankovitch, M.: Kanon der Erdbestrahlung und Seine Andwendung auf das Eiszeitenproblem, Royal Serbian Academy Special Publication, 132, Belgrade, Serbia, 1941.

Niu, L., Lohmann, G., Hinck, S., Gowan, E. J., and Krebs-Kanzow, U.: The sensitivity of Northern Hemisphere ice sheets to
995 atmospheric forcing during the last glacial cycle using PMIP3 models, J. Glaciol., 65, 645–661, https://doi.org/10.1017/jog.2019.42, 2019.

Obase, T., Abe-Ouchi, A. & Saito, F. Abrupt climate changes in the last two deglaciations simulated with different Northern ice sheet discharge and insolation. Sci Rep 11, 22359, https://doi.org/10.1038/s41598-021-01651-2, 2021

Ohmura, A., Calanca, P., Wild, M. and Anklin M.: Precipitation, accumulation and mass balance of the Greenland Ice sheet, Z. Gletscherkd. Glazialgeol., 35(1), 1–20, 1999.

Otto-Bliesner, B. L. and Brady, E. C.: The sensitivity of the climate response to the magnitude and location of freshwater forcing: last glacial maximum experiments, Quaternary Sci. Rev., 29, 56–73, https://doi.org/10.1016/j.quascirev.2009.07.004, 2010.

PAGES Past Interglacials Working Group, o. p.: Interglacials of the last 800,000 years, Rev. Geophys., 54, 162–219, https://doi.org/10.1002/2015RG000482, 2016.

Parrenin, F. and Paillard, D.: Amplitude and phase of glacial cycles from a conceptual model, Earth Planet. Sc. Lett., 214, 243–250, 2003.

Patton, H., Hubbard, A., Andreassen, K., Auriac, A., Whitehouse, P. L., Stroeven, A. P., Shackleton, C., Winsborrow, M., Heyman, J., and Hall, A. M.: Deglaciation of the Eurasian ice sheet complex, Quaternary Sci. Rev., 169, 148–172, https://doi.org/10.1016/j.quascirev.2017.05.019, 2017.

Pattyn, F., Schoof, C., Perichon, L., Hindmarsh, R. C. A., Bueler, E., de Fleurian, B., Durand, G., Gagliardini, O., Gladstone, R., Goldberg, D., Gudmundsson, G. H., Huybrechts, P., Lee, V., Nick, F. M., Payne, A. J., Pollard, D., Rybak, O., Saito, F., and Vieli, A.: Results of the Marine Ice Sheet Model Intercomparison Project, MISMIP, The Cryosphere, 6, 573–588, https://doi.org/10.5194/tc-6-573-2012, 2012.

Pattyn, F., Perichon, L., Durand, G., Favier, L., Gagliardini, O., Hindmarsh, R. C. A., Zwinger, T., Albrecht, T., Cornford, S., Docquier, D., Fürst, J. J., Goldberg, D., Gudmundsson, G. H., Humbert, A., Hütten, M., Huybrechts, P., Jouvet, G., Kleiner, T., Larour, E., Martin, D., Morlighem, M., Payne, A. J., Pollard, D., Rückamp, M., Rybak, O., Seroussi, H., Thoma, M., and Wilkens, N.: Grounding-line migration in plan-view marine ice-sheet models: results of the ice2sea MISMIP3d intercomparison, J. Glaciol., 59, 410–422, https://doi.org/10.3189/2013JoG12J129, 2013.

Pattyn, F.: The paradigm shift in Antarctic ice sheet modelling, Nat. Commun., 9, 2728, https://doi.org/10.1038/s41467-018-05003-z, 2018.

Pausata, F. S. R., Li, C., Wettstein, J. J., Kageyama, M., and Nisancioglu, K. H.: The key role of topography in altering North Atlantic atmospheric circulation during the last glacial period, Clim. Past, 7, 1089–1101, https://doi.org/10.5194/cp-7-1089-2011, 2011.

Peltier, W. R.: The impulse response of a Maxwell Earth, Rev. Geophys., 12, 649–669, https://doi.org/10.1029/RG012i004p00649, 1974.

Peltier, W.: Mantle viscosity and ice-age ice sheet tomography, Science, 273, 1359–1364, https://doi.org/10.1126/science.273.5280.1359, 1996

Pollard, D.: A retrospective look at coupled ice sheet–climate modeling, Climatic Change, 100, 173–194, https://doi.org/10.1007/s10584-010-9830-9, 2010.

Pritchard, H. D., Ligtenberg, S. R. M., Fricker, H. A., Vaughan, D. G., Van Den Broeke, M. R., and Padman, L.: Antarctic ice-sheet loss driven by basal melting of ice shelves, Nature, 484, 502–505, https://doi.org/10.1038/nature10968, 2012.

Quiquet, A., Dumas, C., Paillard, D., Ramstein, G., Ritz, C., and Roche, D. M.: Deglacial Ice Sheet Instabilities Induced by Proglacial Lakes, Geophys. Res. Lett., 48, e2020GL092141, https://doi.org/10.1029/2020GL092141, 2021.

1035 Raymo, M. E. and Mitrovica, J. X.: Collapse of polar ice sheets during the stage 11 interglacial, Nature, 483, 453–456, https://doi.org/10.1038/nature10891, 2012.

Rignot, E. and Jacobs, S.: Rapid Bottom Melting Widespread near Antarctic Ice Sheet Grounding Lines, Science, 296, 2020–2023, https://doi.org/10.1126/science.1070942, 2002.

Ritz, C., Edwards, T. L., Durand, G., Payne, A. J., Peyaud, V., and Hindmarsh, R. C. A.: Potential sea-level rise from Antarctic
1040 ice-sheet instability constrained by observations, Nature, 528, 115–118, https://doi.org/10.1038/nature16147, 2015.

Roe, G. H. and Lindzen, R. S.: The Mutual Interaction between Continental-Scale Ice Sheets and Atmospheric Stationary Waves., J. Climate, 14, 1450–1465, 2001.

Scherrenberg, M. D. W., Berends, C. J., Stap, L. B., and van de Wal, R. S. W.: Modelling feedbacks between the Northern Hemisphere ice sheets and climate during the last glacial cycle, Clim. Past, 19, 399–418, https://doi.org/10.5194/cp-19-399-
1045 2023, 2023.

Schoof, C.: Ice sheet grounding line dynamics: Steady states, stability, and hysteresis, J. Geophys. Res., 112, F03S28, https://doi.org/10.1029/2006JF000664, 2007.

Schoof, C.: Marine ice sheet stability, J. Fluid Mech., 698, 62–72, https://doi.org/10.1017/jfm.2012.43, 2012.

Shepherd, A., Ivins, E., Rignot, E., Smith, B., Van Den Broeke, M., Velicogna, I., Whitehouse, P., Briggs, K., Joughin, I.,
1050 Krinner, G., Nowicki, S., Payne, T., Scambos, T., Schlegel, N., Geruo, A., Agosta, C., Ahlstrøm, A., Babonis, G., Barletta, V., Blazquez, A., Bonin, J., Csatho, B., Cullather, R., Felikson, D., Fettweis, X., Forsberg, R., Gallee, H., Gardner, A., Gilbert, L., Groh, A., Gunter, B., Hanna, E., Harig, C., Helm, V., Horvath, A., Horwath, M., Khan, S., Kjeldsen, K. K., Konrad, H., Langen, P., Lecavalier, B., Loomis, B., Luthcke, S., McMillan, M., Melini, D., Mernild, S., Mohajerani, Y., Moore, P., Mouginot, J., Moyano, G., Muir, A., Nagler, T., Nield, G., Nilsson, J., Noel, B., Otosaka, I., Pattle, M. E., Peltier,
1055 W. R., Pie, N., Rietbroek, R., Rott, H., Sandberg-Sørensen, L., Sasgen, I., Save, H., Scheuchl, B., Schrama, E., Schröder, L., Seo, K. W., Simonsen, S., Slater, T., Spada, G., Sutterley, T., Talpe, M., Tarasov, L., Van De Berg, W. J., Van Der Wal, W., Van Wessem, M., Vishwakarma, B. D., Wiese, D., and Wouters, B.: Mass balance of the Antarctic Ice Sheet from 1992 to 2017, Nature, 558, 219–222, https://doi.org/10.1038/s41586-018-0179-y, 2018.

Siegenthaler, U., Stocker, T. F., Monnin, E., Luthi, D., Schwander, J., Stauffer, B., Raynaud, D., Barnola, J.-M., Fischer, H.,
1060 and Masson-Delmotte, V.: Stable carbon cycle climate relationship during the Late Pleistocene, Science, 310, 1313–1317, 2005.

Sigman, D., Fripiat, F., Studer, A. S., Kemeny, P. C., Martínez-García, A., Hain, M. P., Ai, X., Wang, X., Ren, H., and Haug, G. H.: The Southern Ocean during the ice ages: A review of the Antarctic surface isolation hypothesis, with comparison to the North Pacific, Quaternary Sci. Rev., 254, 106732, https://doi.org/10.1016/j.quascirev.2020.106732, 2021.

1065   Simms, A. R., Lisiecki, L., Gebbie, G., Whitehouse, P. L., and Clark, J. F.: Balancing the last glacial maximum (LGM) sea level budget, Quatern. Sci. Rev., 205, 143–153, https://doi.org/10.1016/j.quascirev.2018.12.018, 2019.

~~Simon, K. M. and Riva, R. E.: Uncertainty Estimation in Regional Models of Long-Term GIA Uplift and Sea Level Change: An Overview, J. Geophys. Res.-Solid Earth, 125, e2019JB018983, https://doi.org/10.1029/2019JB018983, 2020.~~

Spratt, R. M. and Lisiecki, L. E.: A Late Pleistocene sea level stack, Clim. Past, 12, 1079–1092, https://doi.org/10.5194/cp-
1070   12-1079-2016, 2016.

Stap, L. B., van de Wal, R. S. W., de Boer, B., Bintanja, R., and Lourens, L. J.: Interaction of ice sheets and climate during the past 800 000 years, Clim. Past, 10, 2135–2152, https://doi.org/10.5194/cp-10-2135-2014, 2014.

Sueyoshi, T., Ohgaito, R., Yamamoto, A., Chikamoto, M. O., Hajima, T., Okajima, H., Yoshimori, M., Abe, M., O'ishi, R., Saito, F., Watanabe, S., Kawamiya, M., and Abe-Ouchi, A.: Set-up of the PMIP3 paleoclimate experiments conducted using
1075   an Earth system model, MIROC-ESM, Geosci. Model Dev., 6, 819–836, https://doi.org/10.5194/gmd-6-819-2013, 2013.

Sun, S., Pattyn, F., Simon, E. G., Albrecht, T., Cornford, S., Calov, R., Dumas, C., Gillet-Chaulet, F., Goelzer, H., Golledge, N. R., Greve, R., Hoffman, M. J., Humbert, A., Kazmierczak, E., Kleiner, T., Leguy, G. R., Lipscomb, W. H., Martin, D., Morlighem, M., Nowicki, S., Pollard, D., Price, S., Quiquet, A., Seroussi, H., Schlemm, T., Sutter, J., van de Wal, R. S. W., Winkelmann, R., and Zhang, T.: Antarctic ice sheet response to sudden and sustained ice-shelf collapse (ABUMIP), J.
1080   Glaciol., 66, 891–904, https://doi.org/10.1017/jog.2020.67, 2020.

Tabor, C. R. and Poulsen, C. J.: Simulating the mid-Pleistocene transition through regolith removal, Earth Planet. Sc. Lett., 434, 231–240, https://doi.org/10.1016/j.epsl.2015.11.034, 2016.

Tarasov, L. and Peltier, W. R.: Terminating the 100 kyr Ice Age cycle, J. Geophys. Res., 102, 21665–21693, https://doi.org/10.1029/97JD01766, 1997b.

1085   Tarasov, L. and Peltier, W.: Arctic freshwater forcing of the Younger Dryas cold reversal, Nature, 435, 662–665, https://doi.org/10.1038/nature03617, 2005.

Tarasov, L. and Peltier, W. R.: A calibrated deglacial drainage chronology for the North American continent: Evidence of an Arctic trigger for the Younger Dryas, Quaternary Sci. Rev., 25, 659–688, 2006.

Teller, J. T., Leverington, D. W., and Mann, J. D.: Freshwater outbursts to the oceans from glacial Lake Agassiz and their role
1090   in climate change during the last deglaciation, Quaternary Sci. Rev., 21, 879–887, https://doi.org/10.1016/S0277-3791(01)00145-7, 2002.

Sugiyama, S., Minowa, M., Sakakibara, D., Skvarca, P., Sawagaki, T., Ohashi, Y., Naito, N., and Chikita, K.: Thermal structure of proglacial lakes in Patagonia, Journal of Geophysical Research: Earth Surface, 121, 2270–2286, 2016.

~~Shepherd, A., Ivins, E., Rignot, E., Smith, B., Van Den Broeke, M., Velicogna, I., Whitehouse, P., Briggs, K., Joughin, I.,~~
1095   ~~Krinner, G., Nowicki, S., Payne, T., Scambos, T., Schlegel, N., Geruo, A., Agosta, C., Ahlstrøm, A., Babonis, G., Barletta, V., Blazquez, A., Bonin, J., Csatho, B., Cullather, R., Felikson, D., Fettweis, X., Forsberg, R., Gallee, H., Gardner, A., Gilbert, L., Groh, A., Gunter, B., Hanna, E., Harig, C., Helm, V., Horvath, A., Horwath, M., Khan, S., Kjeldsen, K. K., Konrad, H., Langen, P., Lecavalier, B., Loomis, B., Luthcke, S., McMillan, M., Melini, D., Mernild, S., Mohajerani, Y.,~~

Moore, P., Mouginot, J., Moyano, G., Muir, A., Nagler, T., Nield, G., Nilsson, J., Noel, B., Otosaka, I., Pattle, M. E., Peltier, W. R., Pie, N., Rietbroek, R., Rott, H., Sandberg Sørensen, L., Sasgen, I., Save, H., Scheuchl, B., Schrama, E., Schröder, L., Seo, K. W., Simonsen, S., Slater, T., Spada, G., Sutterley, T., Talpe, M., Tarasov, L., Van De Berg, W. J., Van Der Wal, W., Van Wessem, M., Vishwakarma, B. D., Wiese, D., and Wouters, B.: Mass balance of the Antarctic Ice Sheet from 1992 to 2017, Nature, 558, 219–222, https://doi.org/10.1038/s41586-018-0179-y, 2018.

Ullman, D. J., LeGrande, A. N., Carlson, A. E., Anslow, F. S., and Licciardi, J. M.: Assessing the impact of Laurentide Ice Sheet topography on glacial climate, Clim. Past, 10, 487–507, https://doi.org/10.5194/cp-10-487-2014, 2014.

Upham, W.: The geology of central and western Minnesota. A preliminary report. By Warren Upham, assistant on the Geological and Natural History Survey of the state, under the direction of Prof. N. H. Winchell. [From the General Report of Progress for the Year 1879], St. Paul, The Pioneer Press Co., 1880

Uppala, S. M., Kållberg, P. W., Simmons, A. J., Andrae, U., da Costa Bechtold, V., Fiorino, M., Gibson, J. K., Haseler, J., Hernandez, A., Kelly, G. A., Li, X., Onogi, K., Saarinen, S., Sokka, N., Allan, R. P., Andersson, E., Arpe, K., Balmaseda, M. A., Beljaars, A. C. M., van de Berg, L., Bidlot, J., Bormann, N., Caires, S., Chevallier, F., Dethof, A., Dragosavac, M., Fisher, M., Fuentes, M., Hagemann, S., Hólm, E., Hoskins, B. J., Isaksen, L., Janssen, P. A. E. M., Jenne, R., McNally, A. P., Mahfouf, J.-F., Morcrette, J.-J., Rayner, N. A., Saunders, R. W., Simon, P., Sterl, A., Trenberth, K. E., Untch, A., Vasiljevic, D., Viterbo, P., and Woollen, J.: The ERA-40 re-analysis, Q. J. Roy. Meteor. Soc., 131, 2961–3012, 2005.

van Aalderen, V., Charbit, S., Dumas, C., and Quiquet, A.: Relative importance of the mechanisms triggering the Eurasian ice sheet deglaciation in the GRISLI2.0 ice sheet model, Clim. Past, 20, 187–209, https://doi.org/10.5194/cp-20-187-2024, 2024.

van Calcar, C. J., van de Wal, R. S. W., Blank, B., de Boer, B., and van der Wal, W.: Simulation of a fully coupled 3D glacial isostatic adjustment – ice sheet model for the Antarctic ice sheet over a glacial cycle, Geosci. Model Dev., 16, 5473–5492, https://doi.org/10.5194/gmd-16-5473-2023, 2023.

Velay-Vitow, J., Chandan, D., W. Peltier, R.: Into the Holocene, anatomy of the Younger Dryas cold reversal and preboreal oscillation. Sci Rep 14, 3134. https://doi.org/10.1038/s41598-024-53591-2, 2024.

Warren, C. R., Greene, D. R., and Glasser, N. F.: Glaciar Upsala, Patagonia: Rapid Calving Retreat in Fresh Water, Ann. Glaciol., 21, 311–316, https://doi.org/10.3189/S0260305500015998, 1995.

Warren, C. R. and Kirkbride, M. P.: Calving speed and climatic sensitivity of New Zealand lake-calving glaciers, Annals of Glaciology, 36, 173–178, https://doi.org/10.3189/172756403781816446, 2003.

Weertman, J.: Stability of the Junction of an Ice Sheet and an Ice Shelf, J. Glaciol., 13, 3–11, https://doi.org/10.3189/S0022143000023327, 1974.

Yamamoto Willeit, M., Clemens, S.C., Seki, O. et al. Increased interglacial atmospheric CO2 levels followed the mid Ganopolski, A., Calov, R., and Brovkin, V.: Mid-Pleistocene Transition. Nat. Geosci. 15, 307–313 (2022). transition in glacial cycles explained by declining CO2 and regolith removal, Sci. Adv., 5, eaav7337, https://doi.org/10.1038/s41561-022-00918-1 1126/sciadv.aav7337, 2019.
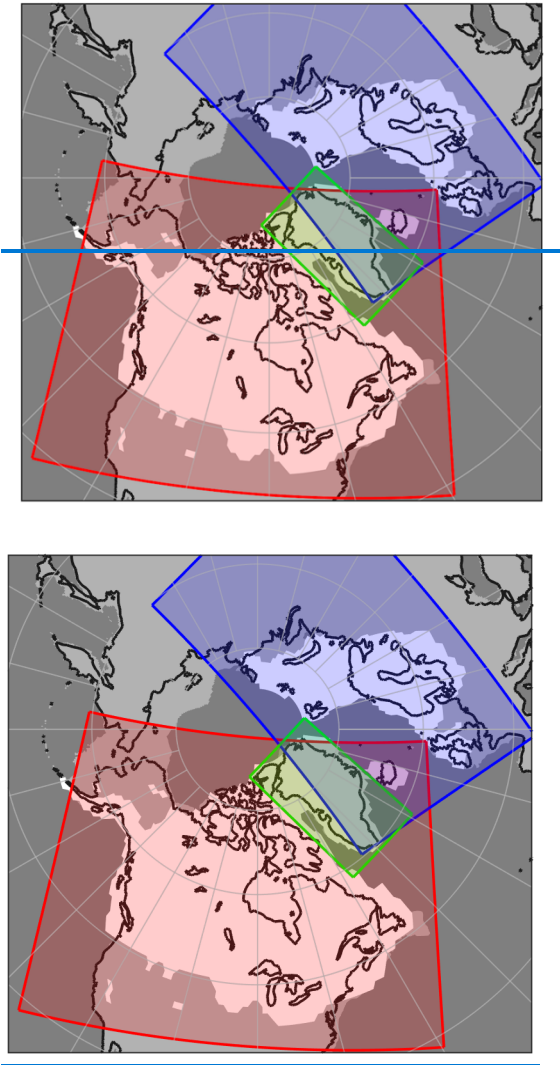
135

Figure 1. The extent of the North American (red), Greenland (green) and Eurasian (blue) domains. The present-day coastline is shown (black lines), as well as the LGM land and ocean (shown in grey). The extent of the LGM ice sheets in Abe-Ouchi et al. (2015) is shown in white.
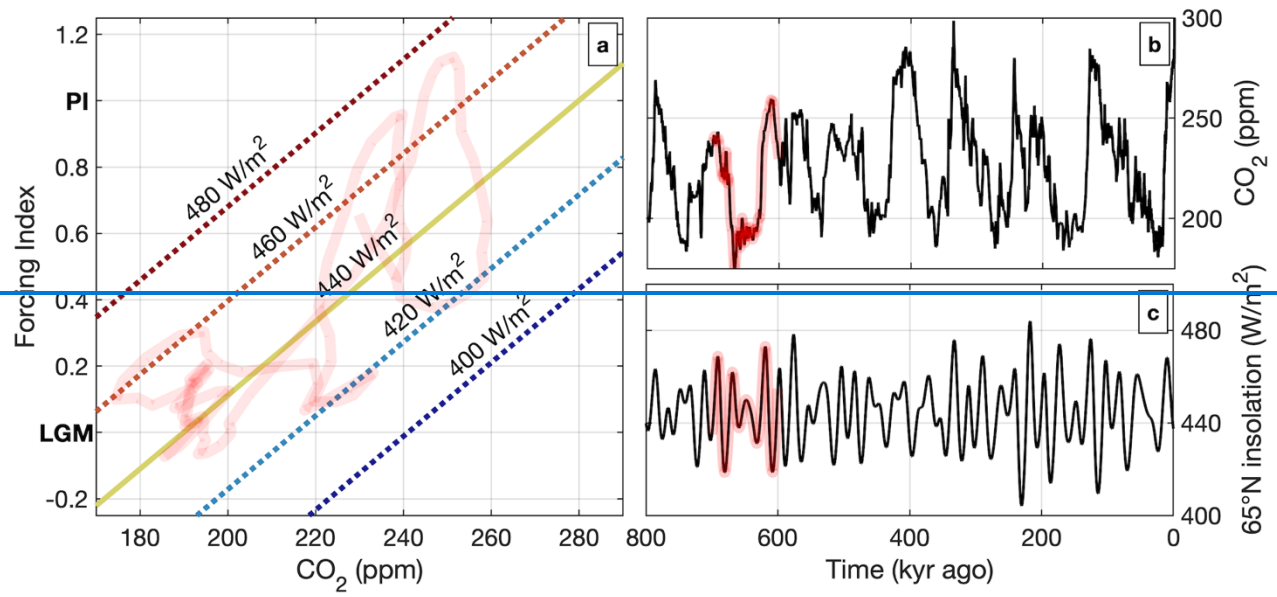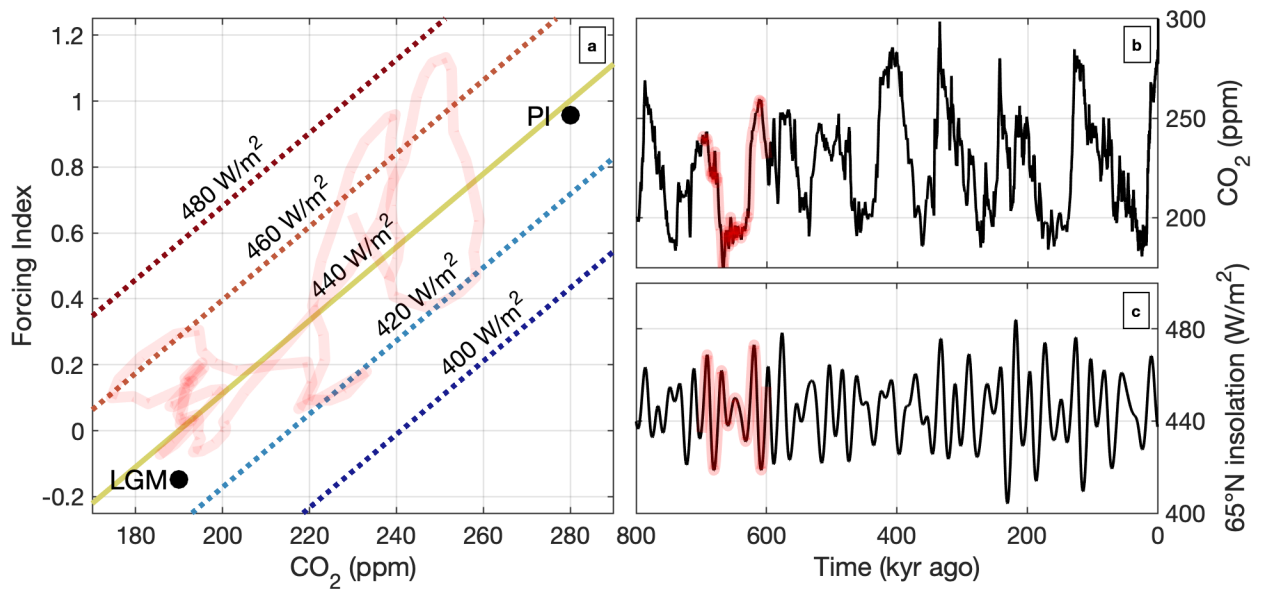
Figure 2. The forcing index (a), which combined with an albedo feedback, drives temperature changes in the ice-sheet model. The forcing index depends on the prescribed CO_2 (b; Bereiter et al., 2015) and insolation (c; Laskar et al., 2004). The pathway of the forcing-index for a 100-kyr period is shown in red. A forcing index of 0 (1) represents LGM (PI) temperature contribution from external forcing.
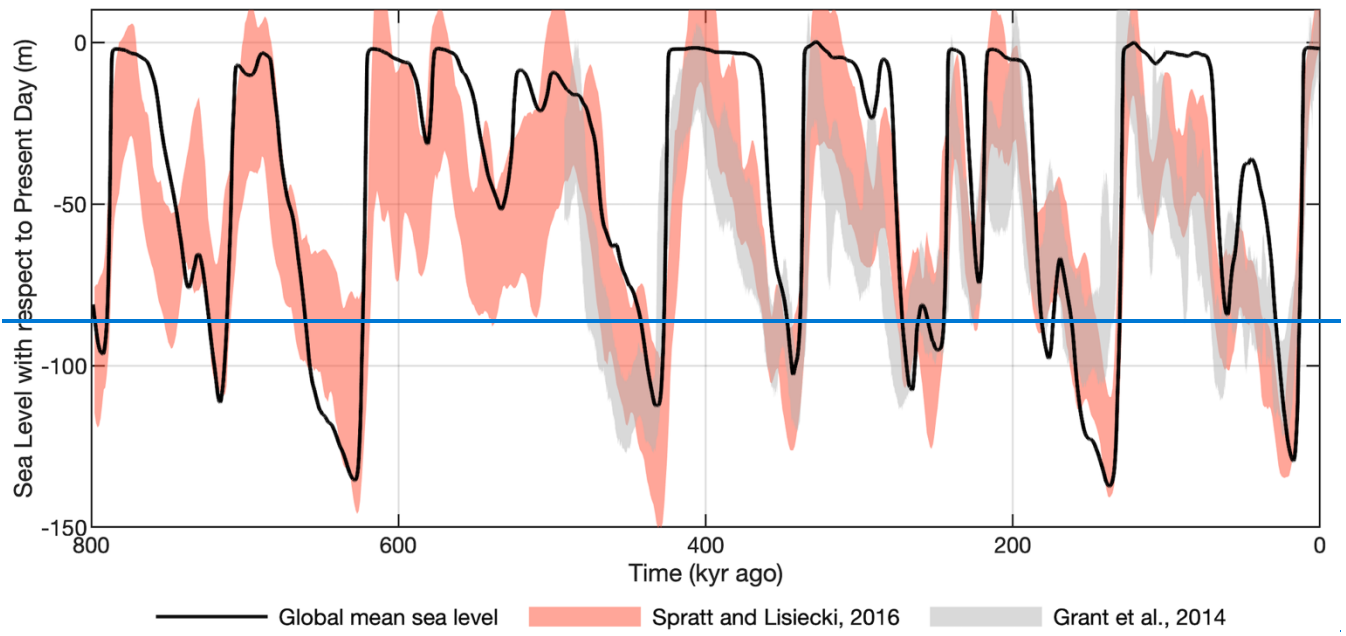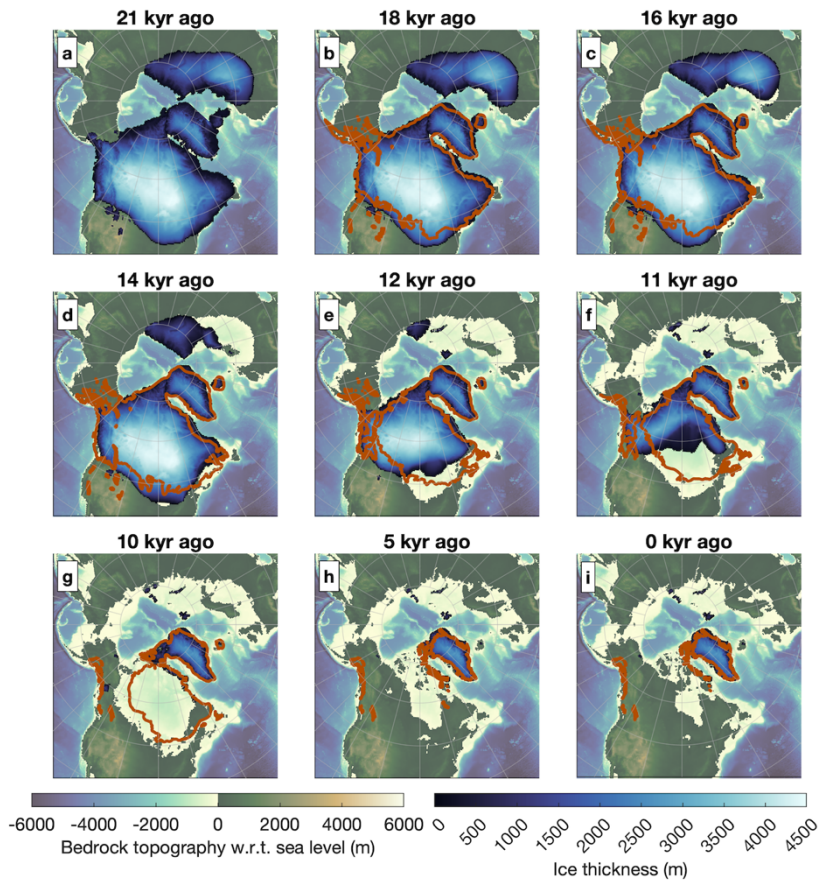
Figure 3. Ice thickness and bedrock topography of the Baseline simulation during the last deglaciation. The reconstruction from Dalton et al. (2020) is shown as orange contours.
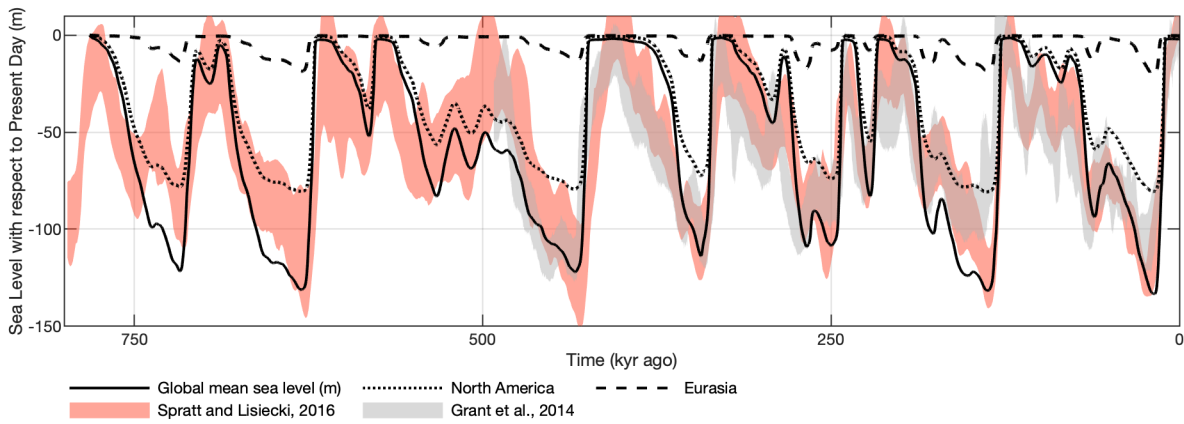
Figure 4. Simulated global mean sea level of North American (dotted line) and Eurasian (dashed line) of the Baseline experiment. Global mean sea level change ~~compared to Grant et al.~~ (solid line) is the volume changed from~~(2014) and Spratt and Lisiecki (2016). 30% was added to~~ the Northern Hemisphere ice sheet ~~volume~~ and an additional 30% to represent other ice sheets (e.g., Patagonia, Himalaya, Antarctica). These are compared to Grant et al. (2014) and Spratt and Lisiecki (2016).
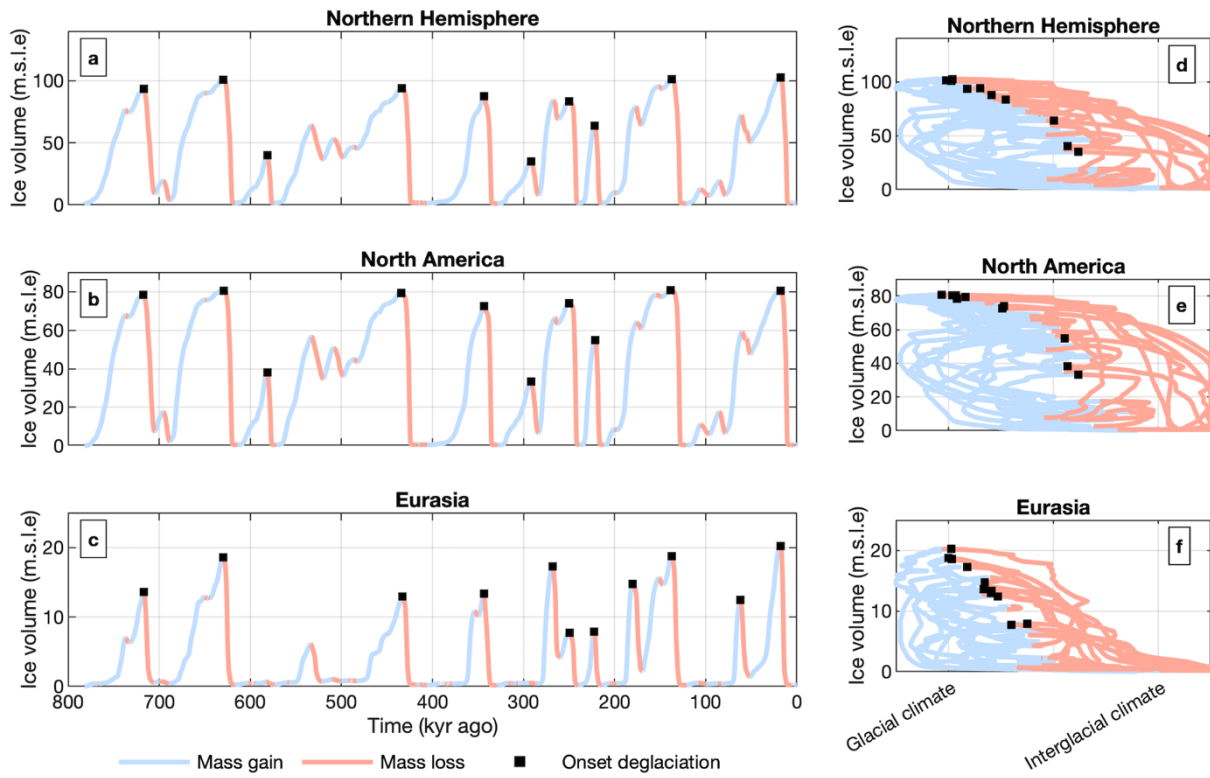
Figure 5. ~~the total sea level change.~~
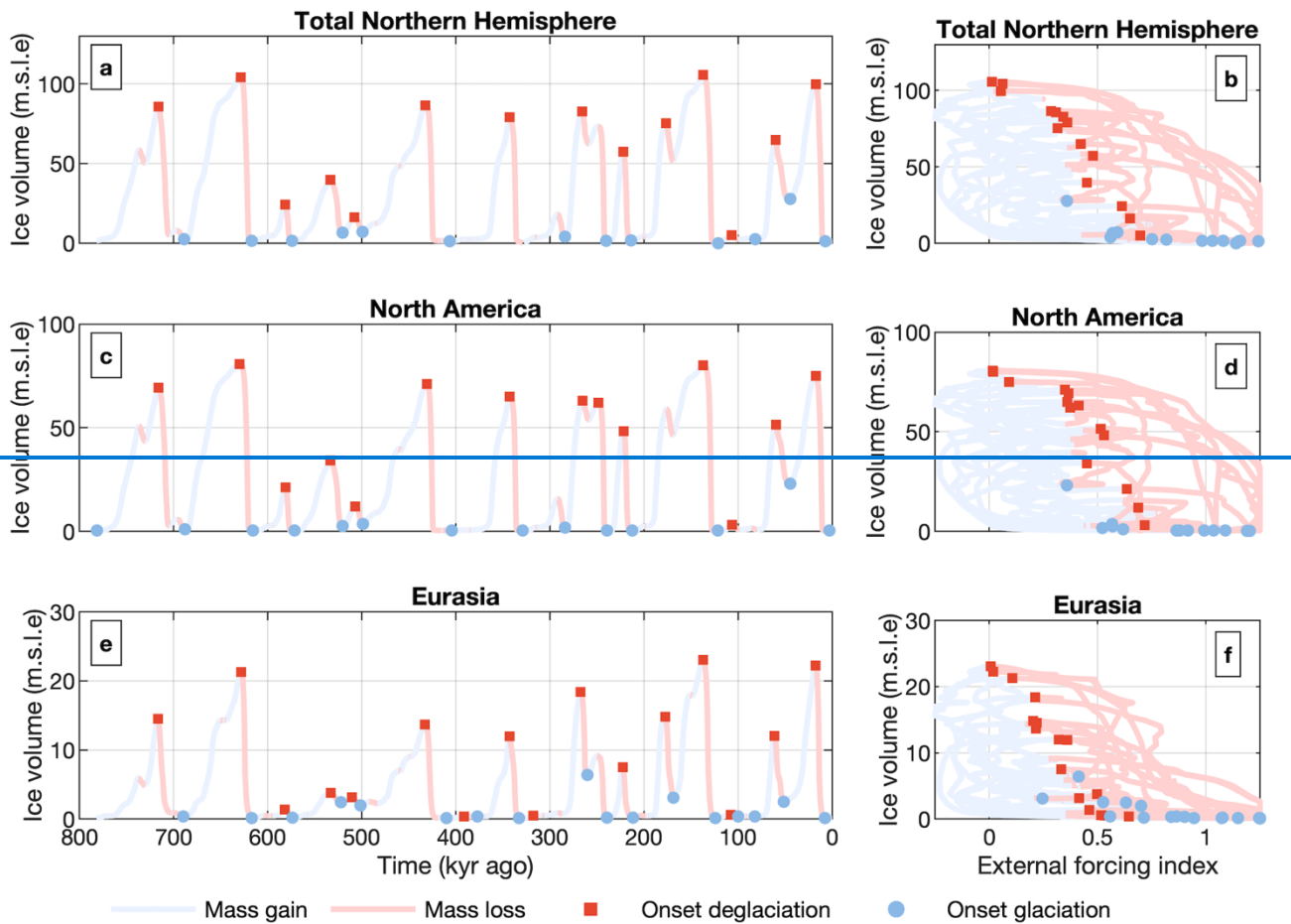
Figure 4. Time series of the simulated ice volume in the Baseline experiment are shown in panels a, c and e. Ice. Panels d-f show the ice volume is compared towith the corresponding climate forcing in the panels c,d and f.(glacial to interglacial) based on the external forcing (prescribed CO_2 and insolation forcing). Panel a,b and c show the ice volume of Eurasia, Greenland and North-America combined, while c, d, e and f only shows one ice sheet per panel. Red colours. Colours indicate when an ice sheet is losing mass, while net melt (red) net accumulation (blue) and onset of deglaciation (black squares). The onset of deglaciation is only placed if the volume is at least 30% at the onset, and lower than 30% by the end of the termination compared to the maximum of the simulation.

1170
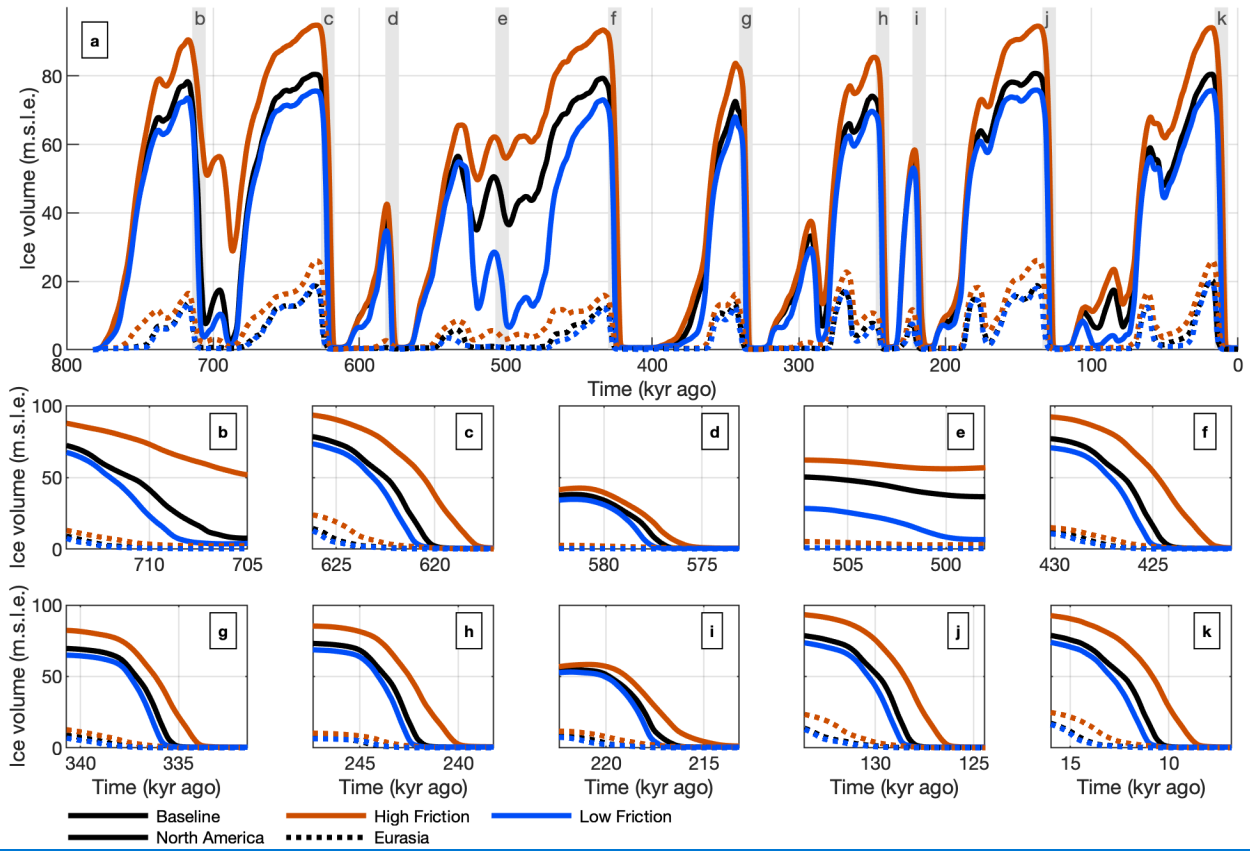
1175 **Figure 6.** ~~shows when an ice sheet gains mass. Blue circles~~ Ice volume (m.s.l.e) time-series of the Baseline, High Friction and Low Friction are shown in panel a. Grey regions in panel a ~~indicate the~~ ~~start of a glaciation, red squares the start of the deglaciation.~~ regions of the zoomed in time-series shown in panels b-k.
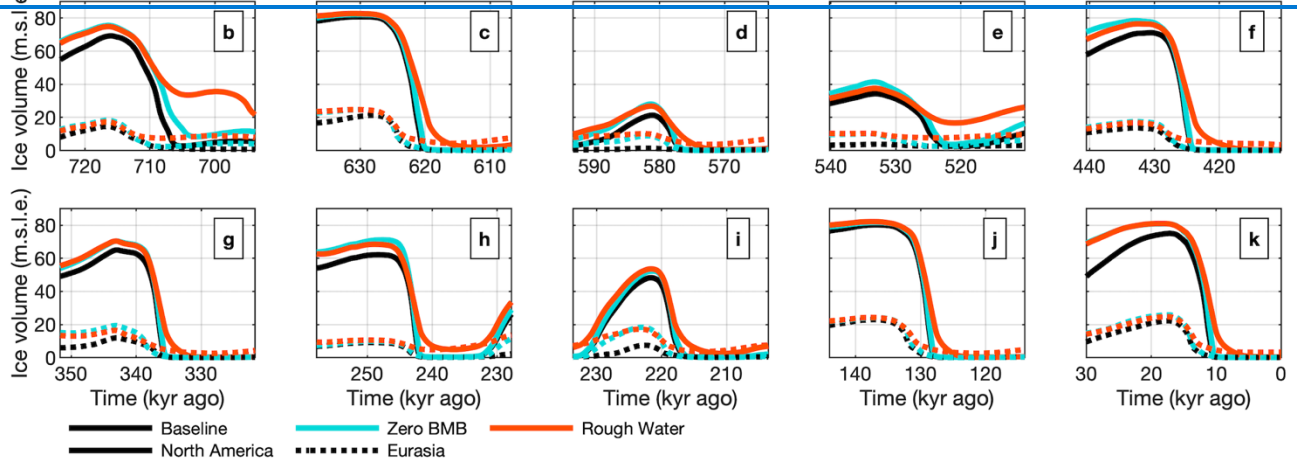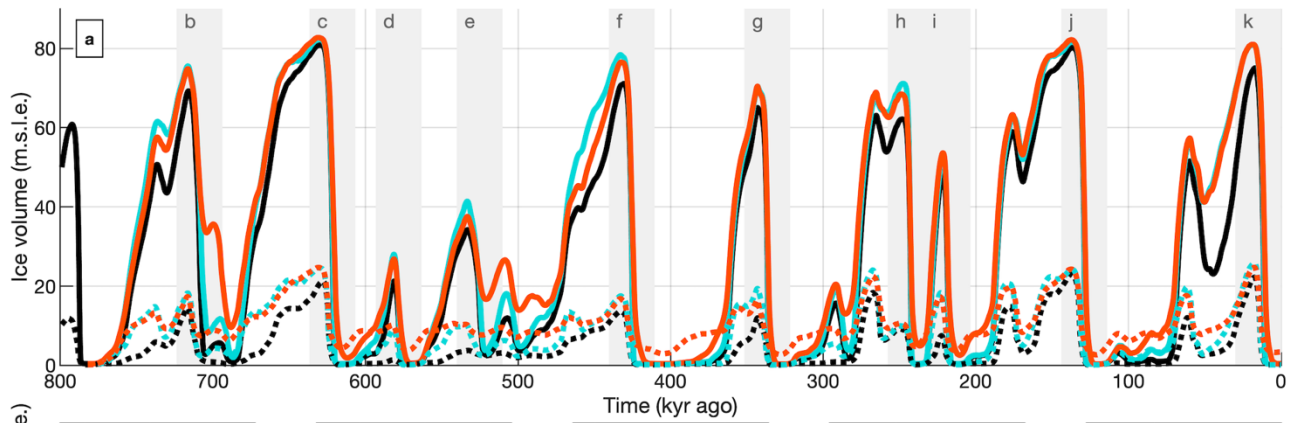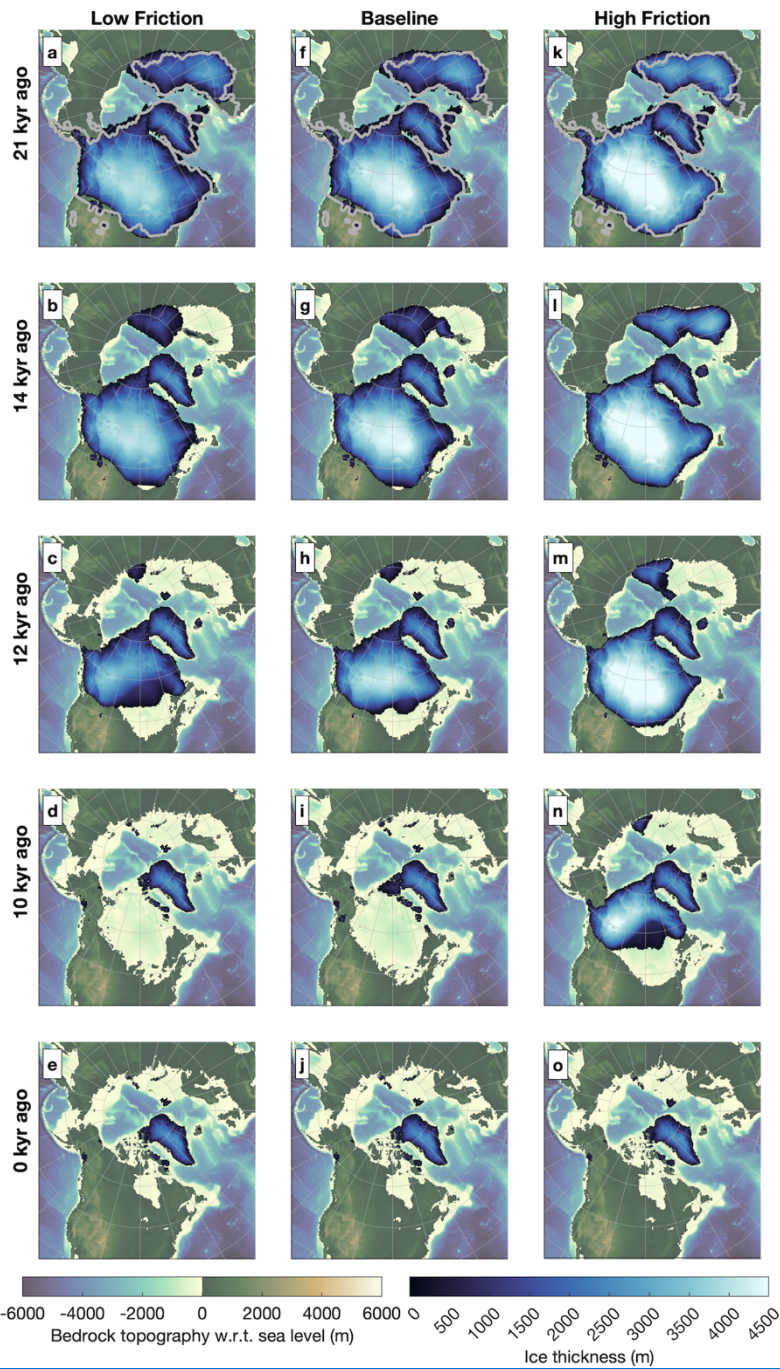
 ~~Figure 5.~~
Figure 7. Ice thickness and bedrock topography of the Low Friction (a-e), Baseline (f-i) and High Friction (k-o) experiments. Time-slices for 21 thousand years ago (kyr; a,f,k), 12 kyr ago (c-m) and 10 kyr (d-n) are shown. The LGM extent from Abe-Ouchi et al. (2015) is shown as grey contours.
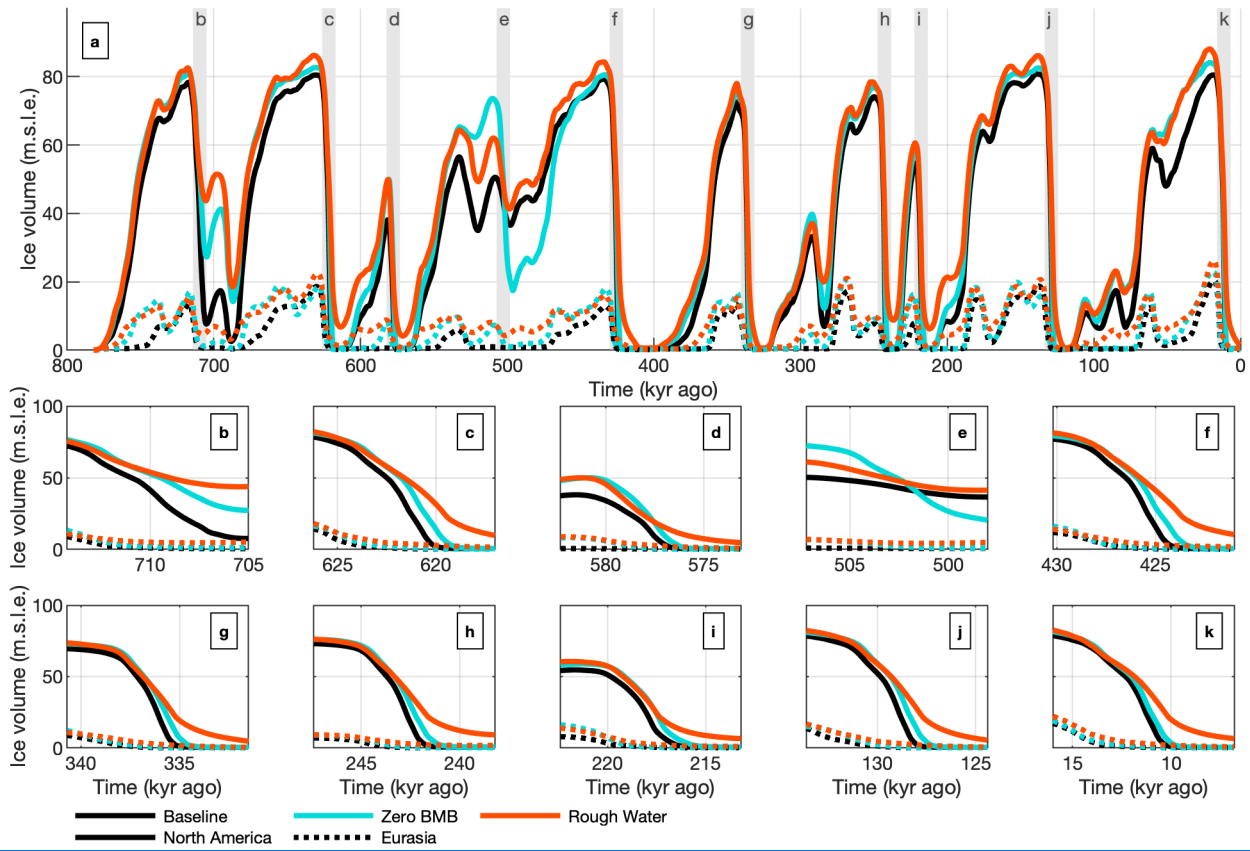
Figure 8. Time-series of the North American and Eurasian ice sheets during various deglacial periods. The full 800 kyr time-series is shown in panel a. The grey patches in panel a correspond to the time-series shown in panels b-k.
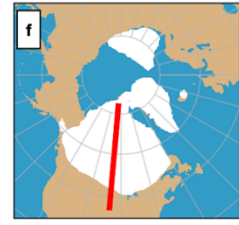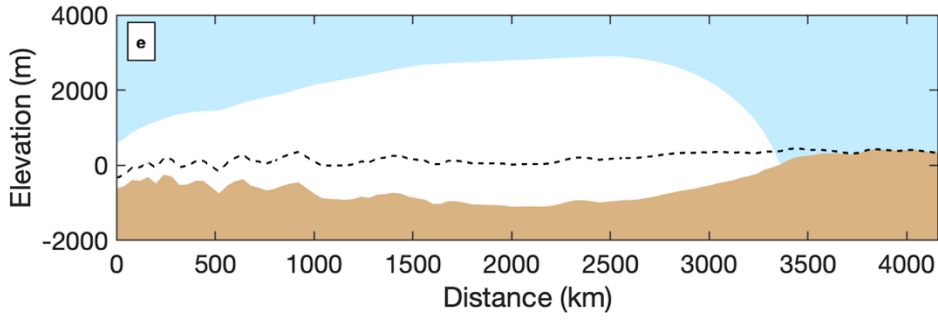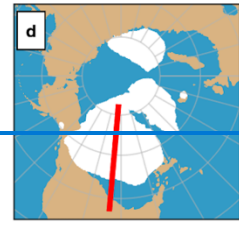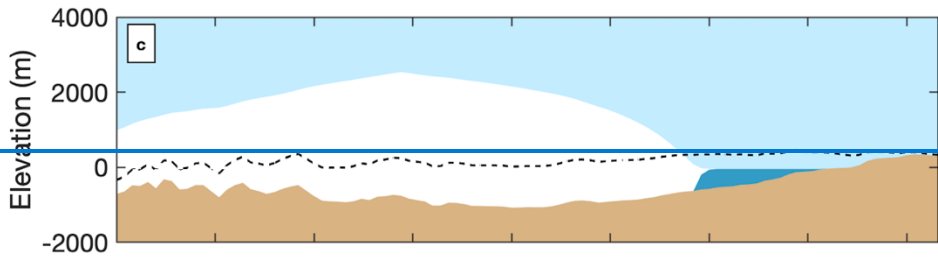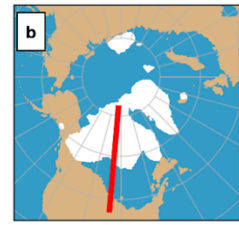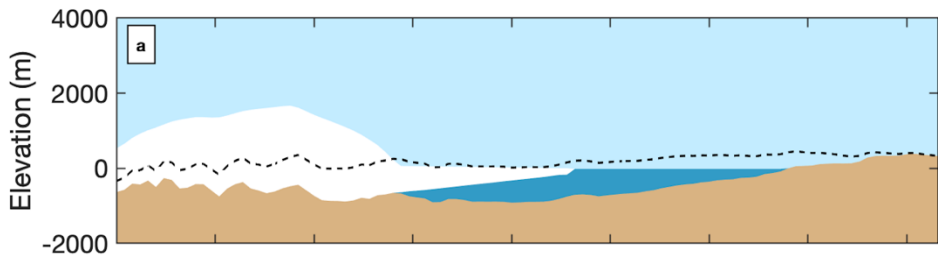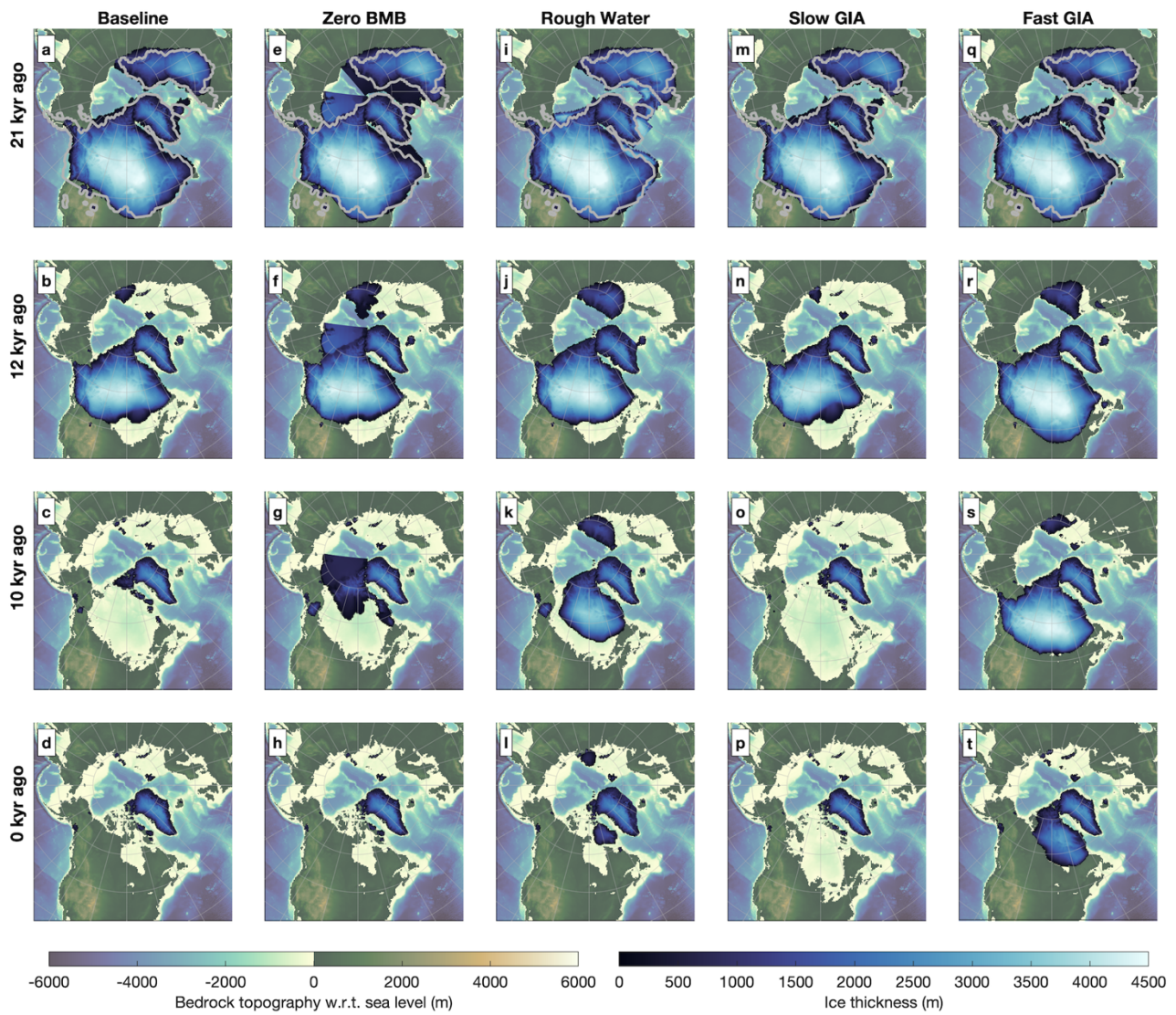
Figure 9. Bedrock topography and ice thickness for the Baseline, Rough Water, Slow GIA and Fast GIA simulations (columns) for 21 ka, 11 ka, 9 ka and 0 ka (rows). The reconstruction from Abe-Ouchi et al. (2015) is shown in grey.
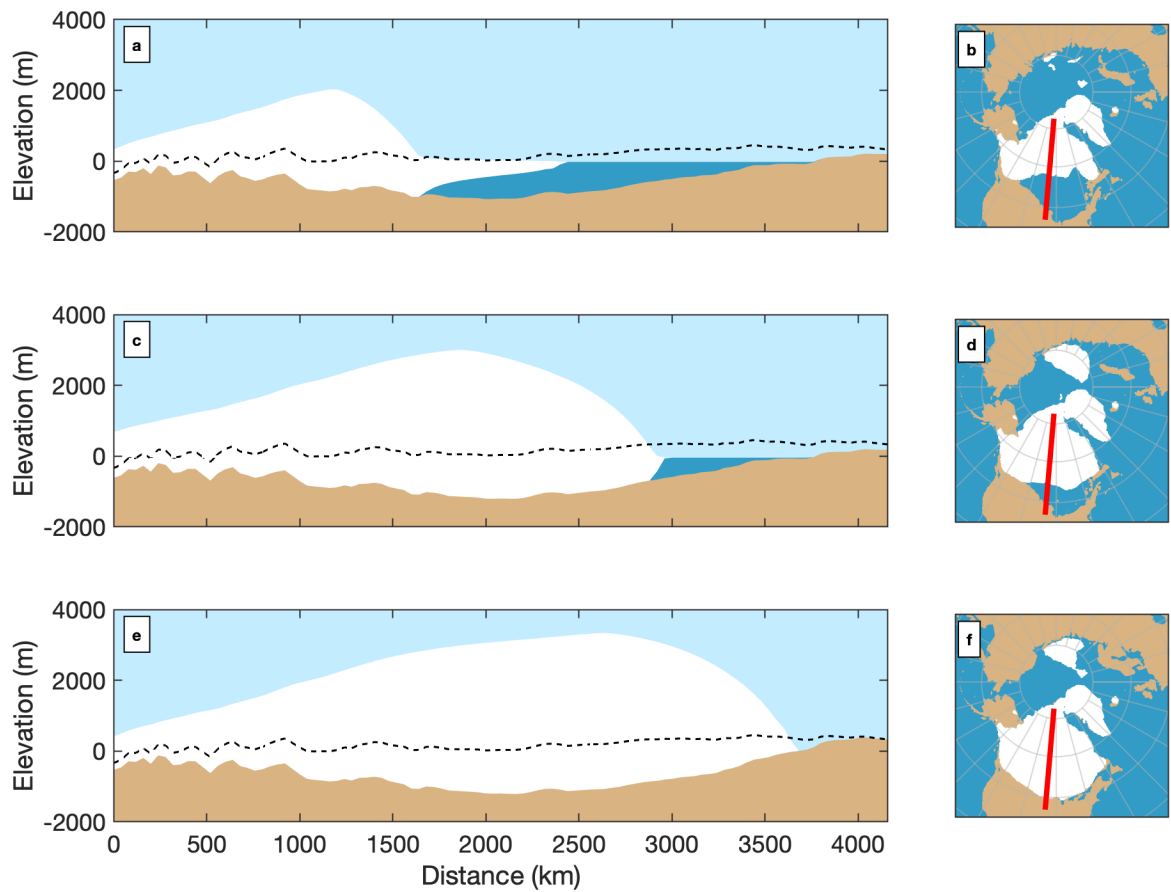
Figure 10.~~Figure 6.~~ Transects (a,c,e) of the Baseline (a,b) the Rough Water (c,d) and Fast GIA simulations (e,f) at 11 kyr ago. ~~PD~~Present-day bedrock is shown as a dashed line in a,c and e. The 0 km distance represents the Northern-most point of the transect, which is shown in ~~figures~~panels b,d and f.

1205
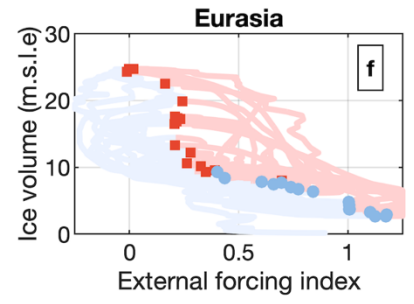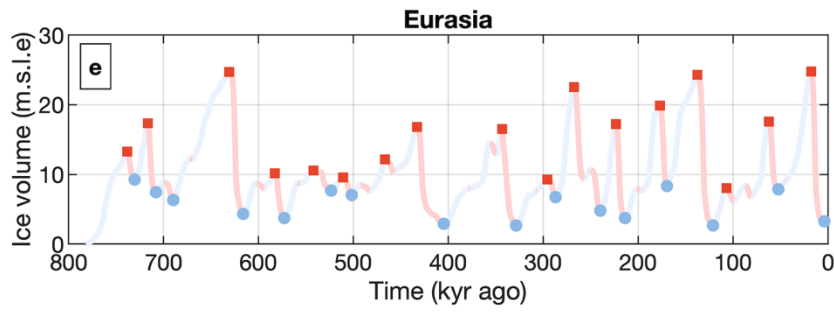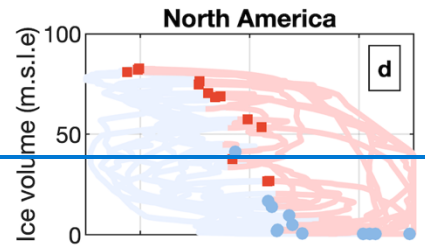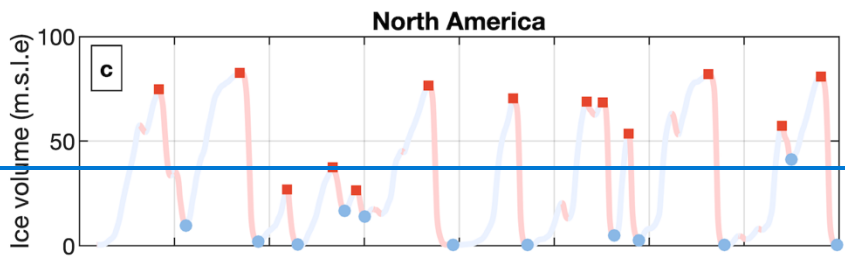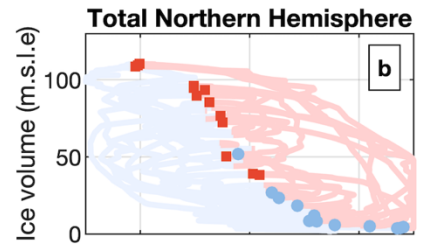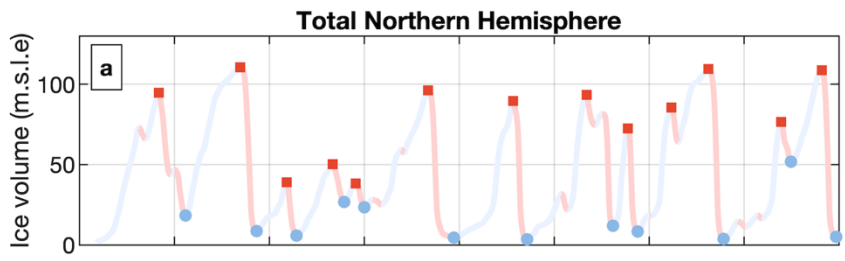
Mass gain   Mass loss ■ Onset deglaciation ● Onset glaciation
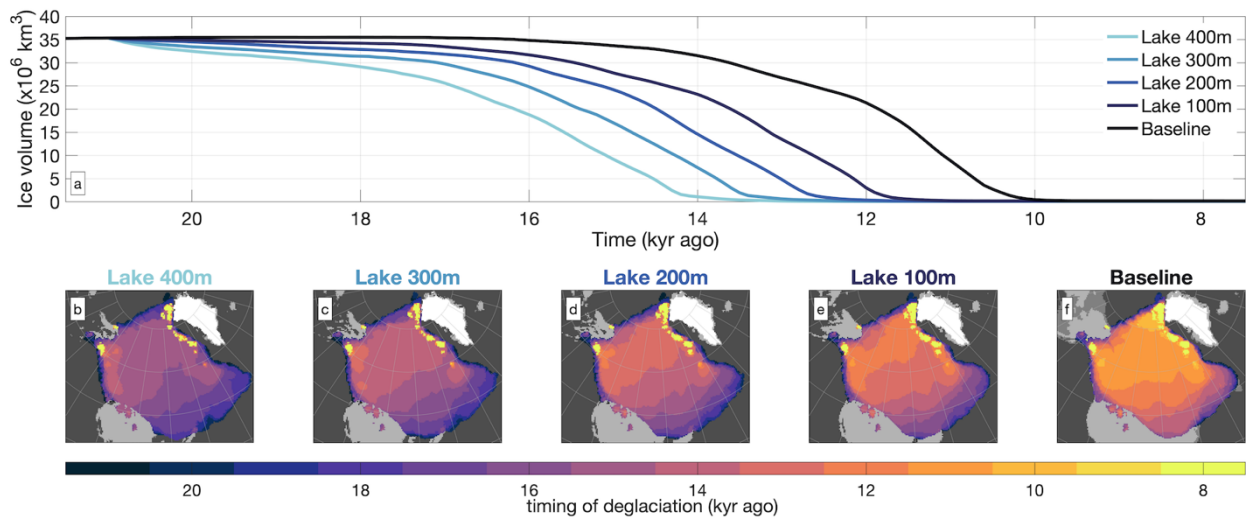
Figure 11. Ice volume time-series of varying lake levels compared to the Baseline. Panels b-f shows the timing of deglaciation. The background colours indicate, from dark to light, ocean during LGM and PI (dark-grey), land during LGM, but not at PI (grey), land in both LGM and PI (light-grey), and the present-day ice coverage (white).
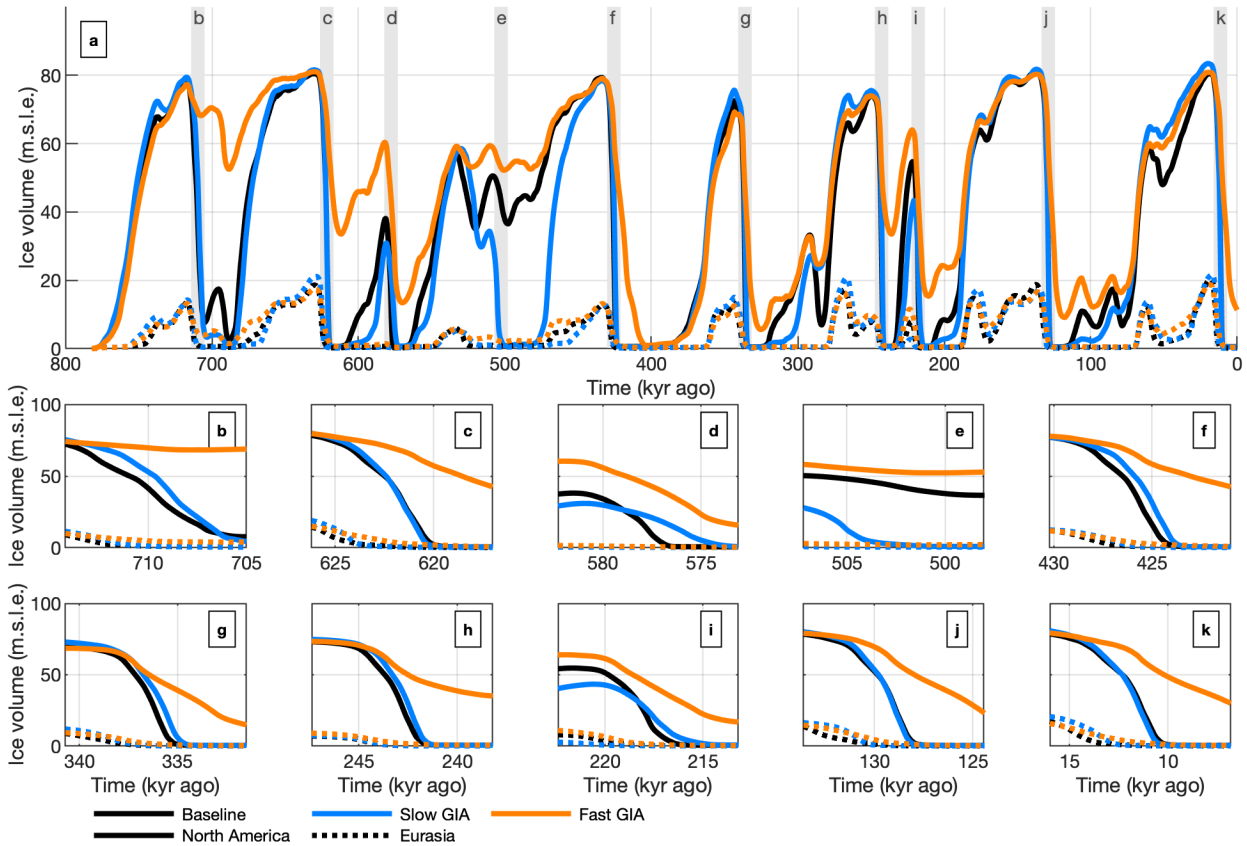
Figure 7. Time series of ice volume from the Rough Water simulation are shown in panels a,c and e. Ice volume is compared to the external forcing for the Rough Water simulation in b,d,f. The Eurasian ice sheet does not melt in the Rough Water simulation, with some ice persisting throughout interglacials in the Barents-Kara Sea region. Red indicates mass loss while blue shows mass gain of the ice sheet. Red squares show the onset of a deglaciation event. Blue circles indicate when the ice sheet starts gaining mass.
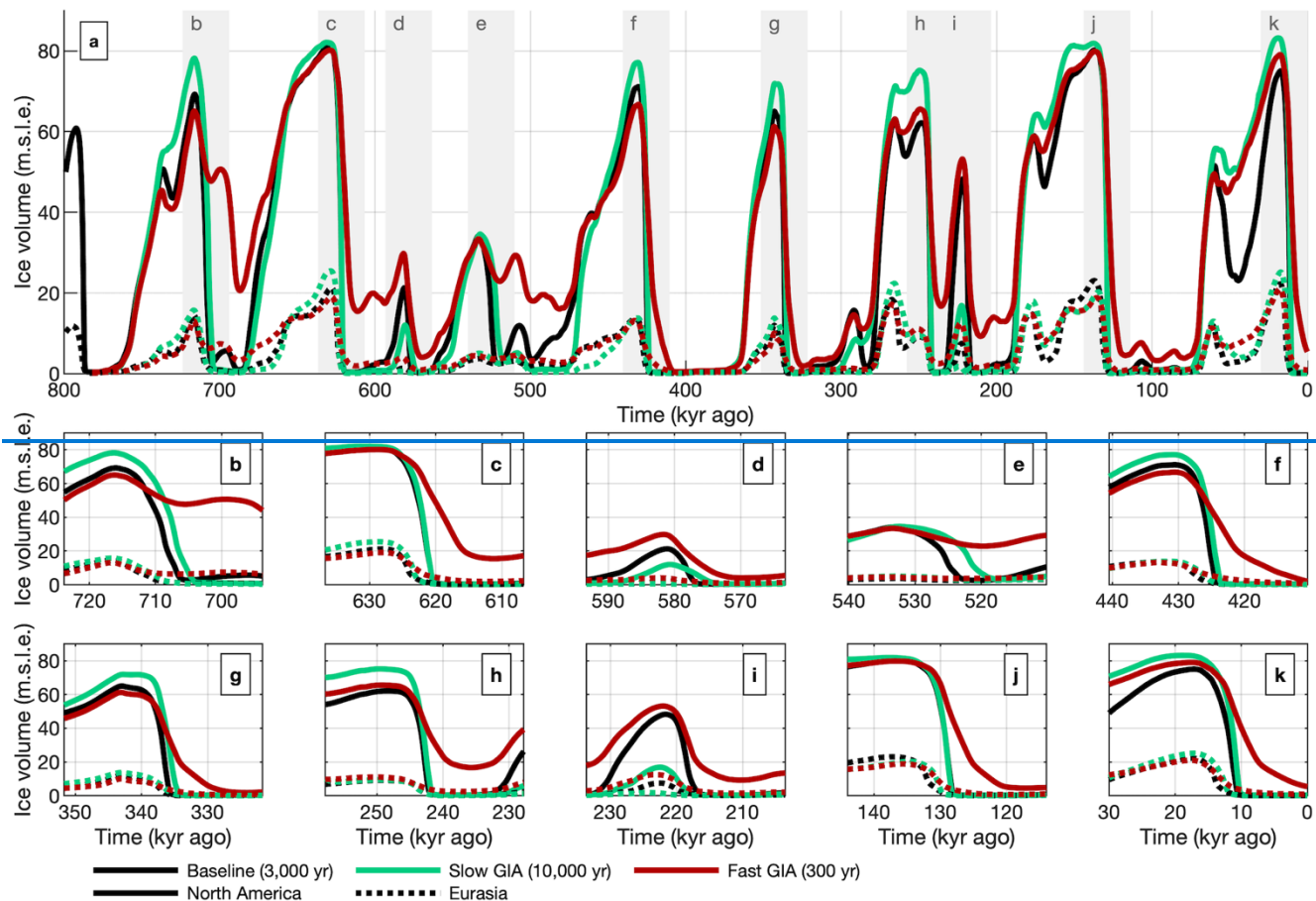
Figure 812. Time-series of ice volume with different GIA relaxation times. The time-series of the past 800 kyr is shown in panel a. Panels b-k show one termination each, which are indicated by the grey patches in panel a.